

# Strategic and practical guidelines for successful structured illumination microscopy

Justin Demmerle<sup>1,8</sup>, Cassandra Victoria Innocent<sup>1,8</sup>, Alison J North<sup>2</sup>, Graeme Ball<sup>1,7</sup>, Marcel Müller<sup>3</sup>, Ezequiel Miron<sup>1</sup>, Atsushi Matsuda<sup>4,5</sup>, Ian M Dobbie<sup>1</sup>, Yolanda Markaki<sup>6</sup> & Lothar Schermelleh<sup>1</sup>

<sup>1</sup>Micron Advanced Bioimaging Unit, Department of Biochemistry, University of Oxford, Oxford, UK. <sup>2</sup>Bio-Imaging Resource Center, The Rockefeller University, New York, New York, USA. <sup>3</sup>Biomolecular Photonics Group, Faculty of Physics, Bielefeld University, Bielefeld, Germany. <sup>4</sup>Advanced ICT Research Institute Kobe, National Institute of Information and Communications Technology, Kobe, Japan. <sup>5</sup>Graduate School of Frontier Biosciences, Osaka University, Osaka, Japan. <sup>6</sup>Department of Biological Chemistry, David Geffen School of Medicine, UCLA, Los Angeles, California, USA. <sup>7</sup>Present address: Dundee Imaging Facility, School of Life Sciences, University of Dundee, Dundee, UK. <sup>8</sup>These authors contributed equally to this work. Correspondence should be addressed to L.S. (lothar.schermelleh@bioch.ox.ac.uk).

Published online 13 April 2017; doi:10.1038/nprot.2017.019

Linear 2D- or 3D-structured illumination microscopy (SIM or 3D-SIM, respectively) enables multicolor volumetric imaging of fixed and live specimens with subdiffraction resolution in all spatial dimensions. However, the reliance of SIM on algorithmic post-processing renders it particularly sensitive to artifacts that may reduce resolution, compromise data and its interpretations, and drain resources in terms of money and time spent. Here we present a protocol that allows users to generate high-quality SIM data while accounting and correcting for common artifacts. The protocol details preparation of calibration bead slides designed for SIM-based experiments, the acquisition of calibration data, the documentation of typically encountered SIM artifacts and corrective measures that should be taken to reduce them. It also includes a conceptual overview and checklist for experimental design and calibration decisions, and is applicable to any commercially available or custom platform. This protocol, plus accompanying guidelines, allows researchers from students to imaging professionals to create an optimal SIM imaging environment regardless of specimen type or structure of interest. The calibration sample preparation and system calibration protocol can be executed within 1–2 d.

## INTRODUCTION

Linear SIM is a powerful and versatile method for generating 3D super-resolution imaging data of biological structures with wavelength-dependent resolution down to ~100–130 nm in lateral dimensions<sup>1,2</sup> and ~280–350 nm in the axial dimension<sup>3,4</sup>. Its efficient optical sectioning capability, rapid multichannel acquisition of live and fixed specimens, compatibility with widely used chemical and biological labels and commercial availability make SIM a popular choice among researchers, with hundreds of instruments being used worldwide. Increasingly easy-to-operate commercial systems have rendered the technique accessible to novice microscopists. However, to generate final super-resolution images, the method relies heavily on complex mathematical algorithms and stringent system calibrations that are ‘black boxes’ to most users. This hidden technical complexity imposes an inherent risk of artifacts with varying degrees of impact that makes reproducibility, adaptation by users and interpretation of biological conclusions difficult, and can undermine confidence in the validity of SIM data<sup>5,6</sup>. The problem is compounded by the absence of widely available resources detailing these artifacts, their causes and how to address them, despite extensive publications detailing principles<sup>7,8</sup>, specific implementations<sup>9,10</sup> and biological applications<sup>11,12</sup> of SIM. Hence, this protocol is designed to facilitate the average researcher in any discipline, as well as imaging facility specialists, in making informed decisions about when and how to use SIM; how to create simple calibration samples to assess and monitor the performance of SIM systems; how to identify and correct for common errors in SIM imaging; and how to effectively present SIM data to the research community. The presented workflow for conducting SIM experiments and assessing data quality and validity should lower entry barriers for the average researcher and reinforce super-resolution microscopy as an essential tool of biological discovery.

## Artifact diagnosis and quality control

The increasing number of publications involving 3D-SIM imaging illustrates the versatility and broad applicability of this method to address important aspects of biological research. However, SIM data presented in research publications commonly show evidence of unreported artifacts that can be misinterpreted as biologically relevant features, potentially leading to false conclusions. In addition to these cases, experience shows that there is a much larger number of undocumented, unsuccessful imaging attempts, particularly when inadequately trained users are approaching the technique with pre-existing samples and without appropriate advice on experimental design and system setup.

Artifacts that may be frequently encountered in typical SIM imaging experiments (Fig. 1) include fine (‘hammerstroke’) pseudo-structures originating from reconstructed nonmodulated background/noise signal that intermixes with poorly resolved structural features (Fig. 1b, Supplementary Fig. 1); echo signals in the axial direction of curved sample structures with different refractive properties (‘lensing’, Fig. 1c); lateral striped extensions (‘hatching’) of features in one or more directions (Fig. 1d, Supplementary Fig. 2); repeated features (‘ghosting’) along the z axis (Fig. 1e, Supplementary Fig. 3); fine hexagonal repeating (‘honeycomb’) pseudo-structures in areas of increased out-of-focus signal, especially in 2D-SIM images (Fig. 1f) or at the end planes of 3D-SIM image stacks (Supplementary Fig. 4); and transfer of signals from features located at opposite ends of the image stack (‘z-wrapping’) (Supplementary Fig. 4). These and other artifacts (a comprehensive list is provided below) often occur concomitantly with a lower-than-expected increase in structural resolution in the lateral and/or axial direction. Attempts to counteract artifacts, either *ex ante* through conservative system hardware settings or *post hoc* through computational filtering,

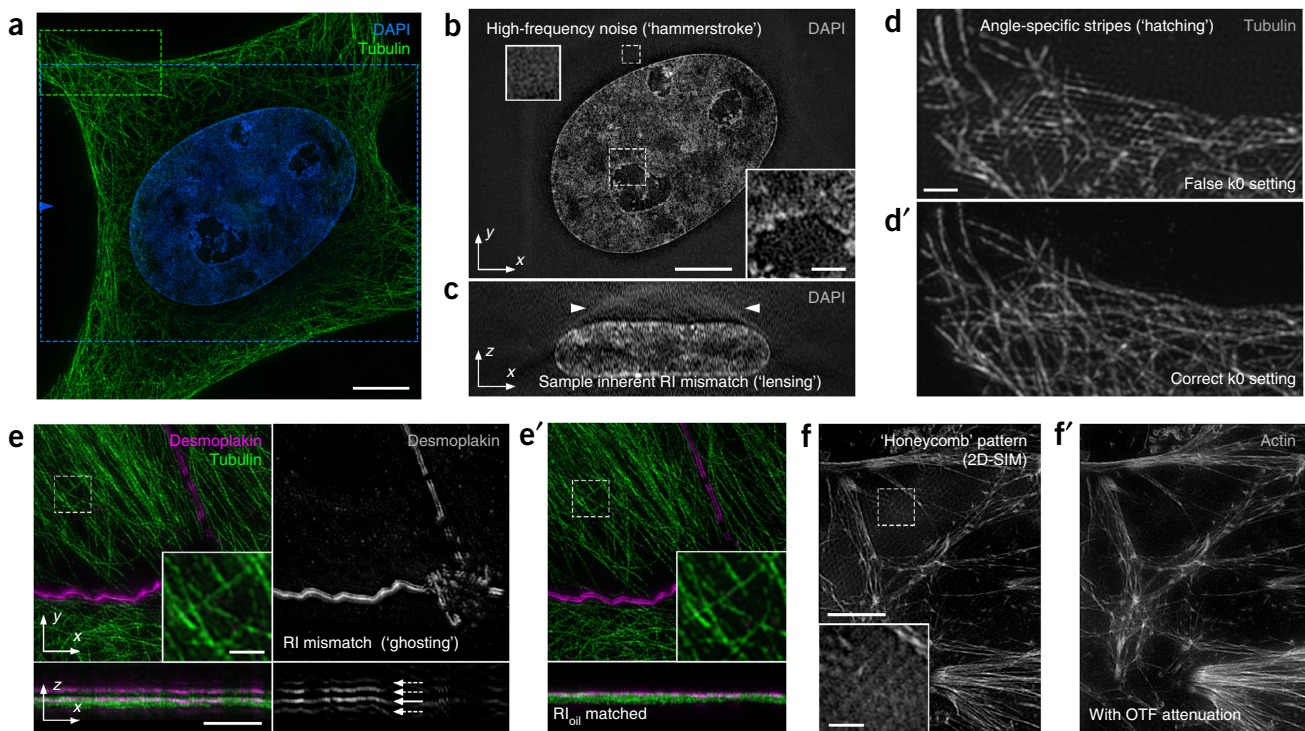


**Figure 1 |** Biological showcase of commonly presented SIM reconstruction artifacts. (a) Maximum z-projection of mouse C127 epithelial cells immunostained for tubulin (Alexa Fluor 488; green), and counterstained with DAPI (blue) exemplifying typical SIM reconstruction artifacts. The blue box denotes the region shown in b, the blue arrowhead denotes the position of the orthogonal view in c and the green box denotes the region shown in d. (b) Optical section of the DAPI-stained nucleus depicted in a. Insets have been expanded to emphasize high-frequency noise contribution, as represented by 'hammerstroke' artifacts, in a background region (small inset) or superimposing genuine features of labeled chromatin (large inset). (c) Orthogonal view demonstrating aberration by a 'lensing' effect caused by a refractive index (RI) mismatch between the stained nucleus and its surroundings (arrowheads). (d) Detailed view of tubulin staining depicted in a, when reconstructed with incorrect angle ( $k_0$ ) settings, leading to 'hatching' of angle-specific stripes intermixed with the genuine tubulin signal. (d') Same region reconstructed with correct angle settings showing no hatching artifact. (e) SIM reconstruction of an MDCK cell immunostained for tubulin (Alexa Fluor 488; green) and desmoplakin C terminus (Alexa Fluor 568; magenta) imaged using an immersion oil whose RI is too low for the sample. Desmoplakin channel only is shown (right) to emphasize the 'ghosting' artifact of structures displaying multiple echo signals along the optical axis (arrows in the orthogonal view). (e') By contrast, when imaged with optimally matched oil, tubulin (green) signals appear sharper (compare insets in lateral views), and only a single layer of desmoplakin (magenta) signal is seen. (f) U2OS cell stained with Phalloidin-ATTO488 for actin and imaged with 2D-SIM, showing 'honeycomb' artifacts as a consequence of out-of-focus blur contribution to the reconstruction (left, inset). (f') Artifacts are reduced by OTF attenuation in the fairSIM reconstruction algorithm (right), which rejects the contribution from out-of-focus signal<sup>44</sup>. Reconstructed images in all panels are shown after thresholding to discard negative intensity values (clipping/baseline subtraction). Scale bars, 5  $\mu$ m and 1  $\mu$ m (insets).

result in images without the expected super-resolution increase, despite greatly improved contrast, thus resembling those obtained by standard wide-field deconvolution microscopy. Thus, it is important to perform quality control checks to confirm the effectively achieved structural resolution in the final reconstructed image, as well as the absence, or sufficient reduction, of artifacts. For an objective assessment of image resolution and data quality, we recommend SIMcheck, which is an open-source plugin for ImageJ/Fiji that provides a collection of raw and reconstructed SIM data checks together with specific calibration tools and useful post-processing utilities<sup>13</sup>. In this protocol, we use SIMcheck along with specifically designed calibration slides as a first step in identifying artifacts and objectively quantifying system performance in order to make informed decisions on how to improve imaging and counteract artifacts.

### Underlying principles

The benefits of SIM, but also its susceptibility to specific artifacts, come from the fundamental concept of the method, which exploits interference effects between a fine-striped illumination

pattern and structures in the sample (analogous to Moiré interference). Through this 'frequency mixing', high spatial frequency components, corresponding to fine details in the sample that would otherwise escape detection, are shifted to collectable lower frequencies in the acquired image. This additional information can be computationally extracted and shifted back to the correct higher frequency before all available information is then recomposed in a linear reconstruction procedure to generate a super-resolution image with up to twice the spatial resolution in all axes (for details on the method, see **Box 1** and **Fig. 2**). The reconstruction algorithm operates in Fourier (frequency, reciprocal) space and relies on the optical transfer function (OTF)—i.e., the Fourier transform of the point-spread function (PSF) that mathematically describes the microscope's response to a fluorescent point source. It works under the premise that the detected light behaves in exactly the same way as in the acquired PSF used to create the OTFs. Therefore, any 'mismatch' between the OTF and the measured sample information will inevitably lead to artifacts of varying severity<sup>3</sup>. In addition to information from the structures of interest, SIM images will also contain information

## Box 1 | The SIM principle

The SIM method takes advantage of the addition of high-frequency information to the image when a fluorescent sample is excited with a periodic fine-striped wide-field illumination. In the case of the original 2D-SIM approach<sup>1,2</sup>, this pattern consists of lateral stripes of a single frequency, with a stripe distance close to the resolution limit of the optical system (i.e., ~200 nm with a 1.4-NA oil immersion objective). These are generated by the interference of two beams of light, which are positioned to enter the objective's back-focal aperture close to opposite edges (+1/-1-order beams). For the more advanced 3D-SIM approach, the illumination pattern is produced by three beams, two outer ones near opposite edges of the back aperture plus a central (0-order) beam. This generates illumination containing two lateral frequencies (first- and second-order stripes of ~400- and ~200-nm width, respectively) and, in addition, an axial modulation near the z-resolution of the optical system, allowing optical sectioning and twofold resolution improvement along the optical axis<sup>3</sup>. The structured illumination pattern interacts with the sample, producing a fluorescent image, which contains information originating from higher spatial frequencies than can usually be observed, corresponding to fine sample details below the diffraction limit. This information is frequency-shifted to lower, observable spatial frequencies and is mixed with the normally visible lower spatial frequencies, an effect similar to the generation of Moiré fringes. Multiple images are collected with the illumination stripe pattern, laterally shifted to different phase positions (typically five steps within the sinusoidal cycle of one wavelength; step size:  $2\pi/5$ ) and rotated (typically in three or five angles with steps of 60° or 36°, respectively). For the super-resolution reconstruction, the data are Fourier-transformed (by fast Fourier transform (FFT)) to convert them to a spatial frequency representation. The information acquired at different phase positions of the SIM stripes produces a set of linear equations to separate the relative contributions from the lower frequencies (equivalent to conventional wide-field imaging) and higher frequencies (the super-resolution information), a step that is also referred to as 'band separation'. The higher frequencies are extracted and shifted to the correct position in frequency space, and different angles are combined to produce a nearly isotropic restoration of the image in the xy dimension. After reconstruction, a generalized Wiener filter is applied to flatten the frequency response with respect to the OTF and compensate for the different relative contribution of fluorescent information and noise. The data are subsequently scaled to more accurately reflect the contribution at different frequencies, using an expanded OTF (i.e., the OTF of a microscope with twice the resolution; referred to as apodization). Finally, the data are inverse Fourier-transformed into real-space information, thus producing a resolution-doubled image. **Figure 2a** illustrates these steps for a three-beam interference illumination, as required for 3D-SIM reconstructions, in spatial and frequency space. A simulation of the reconstruction process illustrating the generation of high-frequency information (for simplicity, only one dimension using a two-beam interference illumination is depicted) is shown in **Figure 2b**.

Reconstructed super-resolution SIM images not only feature up to eightfold (3D-SIM) improved volumetric resolution, but also combine this with strong contrast enhancement (in the orders of magnitude) because of effective rejection of out-of-focus signal, as well as very efficient frequency transfer in the 100- to 200-nm resolution range<sup>4,5</sup>. Of note, the reconstruction uses mostly linear processing<sup>3</sup>, and mixes original and shifted frequencies in real space, thus retaining relative intensity differences for subsequent quantitative analyses.

Importantly, recombining the different spatial frequency components requires good knowledge of the amplitude at which the optical system transfers this information. This is usually extracted from the system's OTF. Only when the system's OTF and the sample properties during acquisition are reasonably matched will the reconstruction algorithm produce valid results, virtually free from notable artifacts. Irregularities such as spherical aberration substantially affect the amplitude of information transfer with spatial frequency, and hence the quality of reconstructions, as the computational algorithm can no longer properly match the intensity of different components during processing.

Another critical factor is the amplitude of the stripe modulation in the collected images. The stripes enable the shifting of uncollectable high spatial frequency information to lower, collectable frequencies. The contrast of these stripes is directly linked to the amount of retrievable high-frequency information. **Figure 2c** illustrates this relationship in a simulation of SIM reconstructions at different modulation depths and background levels. In the extreme case of no stripe contrast, the image is simply a conventional (diffraction limited) wide-field image that, depending on the Wiener filter setting, is more or less interwoven with the characteristic 'hammerstroke' pseudo-structure from reconstructing unmodulated noise (**Fig. 1b, Supplementary Fig. 1**). By using the 'modulation contrast/modulation contrast map' functions in SIMcheck, the stripe modulation can be measured and mapped to the reconstructed data, enabling assessment of regions where SIM has worked well and where it has not (**Fig. 3, Supplementary Fig. 1**). Increasing the Wiener filter constant reduces reconstructed noise artifacts, albeit at the expense of blurring the reconstructed image and thereby (seemingly) reducing its resolution. However, in raw SIM data with lowered modulation contrast, high-resolution information is less likely to be present, and therefore increasing the Wiener filter generates a more realistic representation of the 'effective' achievable resolution. Furthermore, Wiener filtering should be applied sparingly, as overfiltering generates other characteristic artifacts (visible as cartwheel-shaped Fourier plots). Importantly, no filtering can ever compensate for low SNR/modulation contrast in the input data, and can only reduce detrimental effects to a small extent.

Finally, the resolution improvement achieved in SIM relies on both a fine spacing and a high-modulation depth for the excitation light pattern. Therefore, a coherent light source (i.e., a laser) capable of introducing destructive interference in the pattern is required for maximum contrast and thus best performance. Incoherent light sources (such as LEDs) can be used only when compromises in resolution improvement or SNR are acceptable.

from other sources, including optical aberrations in the sample, nonspecific labeling or noise, all of which can distort or obscure the structures of interest in the reconstructed image. Moreover,

systematic aberrations can also be generated if the optical condition of the illumination pattern and its interaction with the sample are suboptimal.

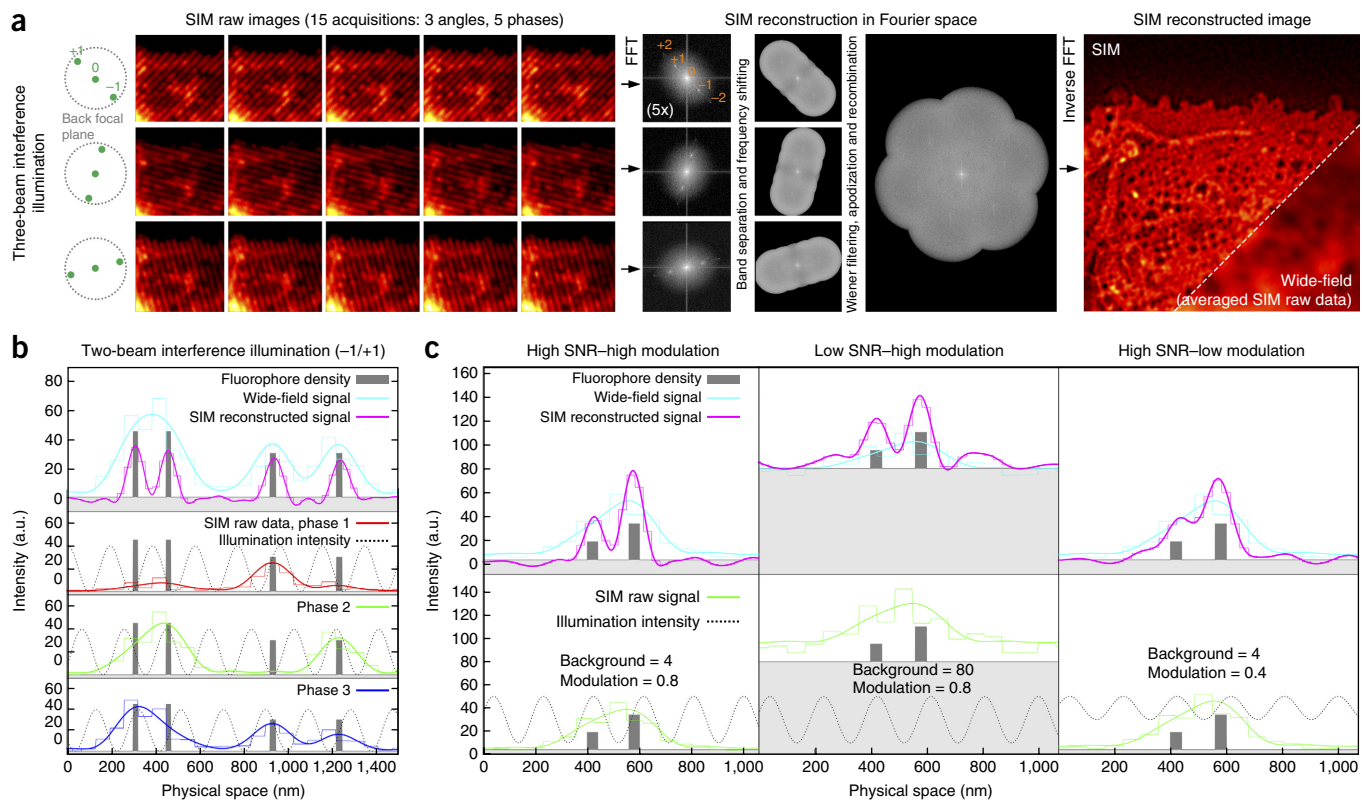


**Figure 2 |** Principle of extending resolution with structured illumination (SI). **(a)** Illustration of SIM image acquisition and processing steps, as described in detail in Box 1. Example data showing small pores (fenestrae) in a subregion of a membrane-stained liver endothelial cell<sup>19</sup>. **(b)** Simulation of the reconstruction process illustrating the generation of high-frequency information. For simplicity, only one dimension using a two-beam interference illumination with three phase steps is shown, with the y axis representing arbitrary intensity units, and the x axis representing physical space in nanometers. For each setting of the illumination pattern phase (dotted gray line in the lower three diagrams), different areas of the ‘1D sample’ containing two bright and two less bright emitters (gray bars, 40 nm wide) are excited, which generate three different signal responses (red, green and blue curves, fitted to 64-nm pixel intensities represented by thinner angular lines underneath). Using this extra information, close-by ‘fluorophores’ (two gray bars on the left side), indistinguishable in wide-field, can be separated after the SIM reconstruction (upper panel, cyan and magenta curves; underlying pixel width 64 and 32 nm, respectively). The contrast between emitters that are just resolvable in wide-field (two gray bars on the right, spaced close to the resolution limit) also improves, whereas relative signal intensity differences between single emitters are preserved. **(c)** Simulation of SIM reconstructions at different modulation depths and background levels (indicated by solid gray line). High modulation and high sample SNR with low background yields a high-quality reconstruction (**c**, left; high contrast separation of the two emitters, linear relationship of their intensities). For high-modulation depth, but low sample SNR (e.g., with increased out-of-focus background), additional shot noise enters the reconstruction and degrades image quality (**c**, middle). For high sample SNR, but low SIM pattern contrast, the resolution improvement becomes hardly noticeable (**c**, right).

Importantly, practical achievement of the theoretical resolution enhancement depends profoundly on the contrast of the illumination stripes on the sample features. We generally refer to this as ‘modulation contrast’, which is determined both by the contrast properties of the labeled sample features and the optical properties and ‘stripe quality’ of the instrument<sup>13,14</sup> (Box 1, Figs. 2c and 3). In the extreme case of no modulation contrast, no interference (super-resolution information) is present and therefore resolution is not enhanced at all. In a more general case, if the modulation contrast is reduced, a smaller-than-expected fraction of the data can be derived from the high-frequency features, reducing contrast and decreasing super-resolution image quality and information content. Major contributions to this effect in biological samples are low contrast (signal-to-noise ratio (SNR)), either inherent to the sample or from suboptimal labeling, and spherical aberration caused by refractive index (RI) mismatch between the immersion media, mounting media and the sample. The improvement of modulation contrast, by increasing specific

signal intensity over nonspecific background, and by optimizing RI matching through choice of immersion medium, is the aspect of SIM that the average user can perform relatively easily (as altering fundamental hardware and software properties is usually not possible) and is emphasized for that reason.

Consequently, there are two important principles to consider when designing and executing SIM experiments. The first, which is the main focus of this protocol, is to ensure that the illumination pattern is consistent, highly contrasted and optimally calibrated, and that it matches the OTF used for the mathematical reconstruction. This is accomplished by regularly confirming microscope calibration and by correcting for (depth-dependent) spherical aberrations caused by RI mismatch between the coverslip, mounting medium and specimen. The second principle involves minimizing signal originating from sources other than the structure of interest, through careful experimental design and heightened standards for sample preparation and image acquisition. These aspects are discussed in the accompanying protocol by Kraus *et al.*<sup>15</sup>.

# PROTOCOL

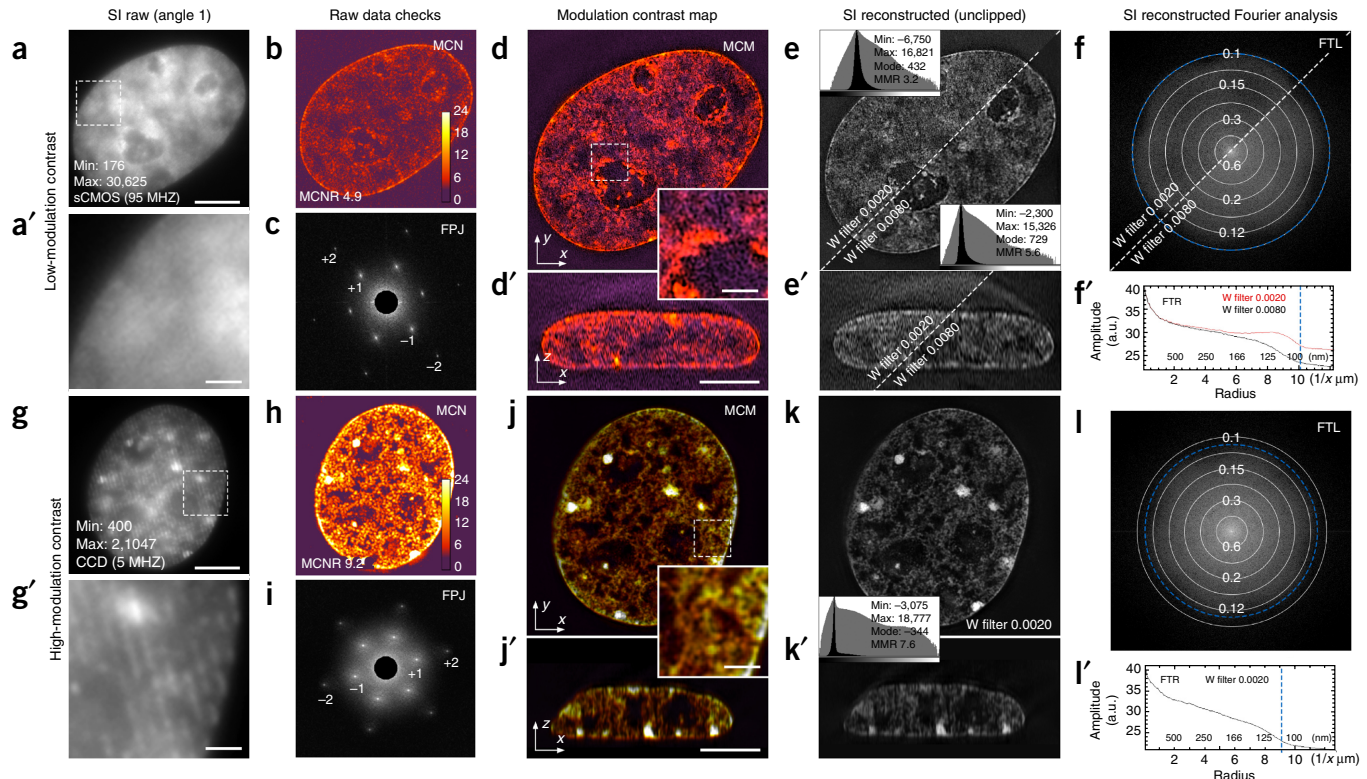


**Figure 3 |** Identifying differences in modulation contrast. DAPI-stained C127 cells with either low-modulation contrast (**a**) or high-modulation contrast (**g**), and the resulting diagnostic readouts (upper two rows and bottom two rows) from SIMcheck. The left-most column shows representative raw data (**a** and **g**) with intensity minima, maxima and camera type (top), and insets below (**a'**,**g'**) show near absence or presence of structured illumination pattern imposed on the sample's signal. The second column shows raw data checks: (**b**,**h**) modulation contrast to noise (MCN) output from SIMcheck of a single frame of the image stack, with each pixel assigned a heatmap value, and the average modulation contrast to noise ratio (MCNR) value for the image noted in the bottom left corner. (**c**,**i**) Maximum intensity projection of the fast Fourier transform (FFT) of the raw data ('Fourier Projection (FPJ)' output from SIMcheck), showing less extended cloud of high-frequency information and slightly weaker second-order spots from the low-modulation contrast data. Third column: lateral (**d**,**j**) and orthogonal (**d'**,**j'**) views of the reconstructed images superimposed with the MCN map shown previously (MCM), illustrating the difference in reconstruction output as a function of modulation contrast in the raw image. Boxed insets show details of chromatin. Purple and dark red features highlight reconstructed pseudo-structures with low underlying modulation contrast, which are not considered trustworthy. Fourth column: nonthresholded lateral (**e**,**k**) and orthogonal (**e'**,**k'**) views of the reconstructed image. In **e** and **e'**, reconstruction results for using low and high Wiener (W) filter settings are displayed side by side separated by a dashed diagonal line. Corresponding intensity histograms of reconstructed stacks, with respective intensity minima, maxima, modes and the minimum-to-maximum ratio (MMR), are displayed as insets. Values of assigned floating-point data are displayed as log-scale (gray) and linear-scale (black) histograms from the 'Reconstructed Intensity Histogram' (RIH) output of SIMcheck. (**f**,**l**) Reciprocal-space images of log-scaled 3D FFT of reconstructed data, with correlated dimensions in real space superimposed as rings and denoted in microns, from the 'Fourier Transform Lateral (FTL)' output from SIMcheck. (**f'**,**l'**) Corresponding radial profile of amplitude component from the 3D FFT of reconstructed data 'Fourier Transform Radial (FTR)' output from SIMcheck. Amplitude is indicated in arbitrary units on the y axis, and reciprocal distance on the x axis, denoted either in tenths of a micron or nonreciprocally in nanometers (SIMcheck). Note the difference in shape of the FTR plots between low-modulation contrast data (with either a low or high Wiener filter setting) and high-modulation contrast data. Generally, a flat central profile together with steep drops at the center and toward the edge of the theoretical frequency/resolution limit (indicated by blue dashed circle and line in the FTL and FTR at ~100 nm and ~110 nm, respectively) is indicative of a poor reconstruction, whereas a more straight-line decline is indicative of high data quality. Note also that the relative quality difference correlates with both MMR and MCNR values. Scale bars, 5 μm and 1 μm (insets).

## Overview of the procedure

In addition to existing recommendations, experimental researchers have noted the need for a broad and accessible set of guidelines to improve experimental design, confirm instrument calibration and assess image data quality<sup>16,17</sup>. Although specifics may vary across system manufacturers, sample types and the nature of the experiments, here we offer a calibration sample procedure, artifact diagnosis and reference tables as a roadmap to more accessible high-quality data collection and interpretation on a range of current SIM systems. As specified above, examples of the most common SIM-related artifacts are introduced to exemplify what the inexperienced user may encounter (Fig. 1, Supplementary Figs. 1–4). The critical concept of modulation contrast as a

predictor and metric of SIM data quality is illustrated in Figure 3, as maximizing this property in both system and sample is the goal of these calibration routines, as well as the key to achieving reliable data.

Once these central issues are presented, the user is encouraged to re-evaluate the general imaging strategy in terms of microscopy technique, instrumentation and their suitability for addressing a specific biological research question (Supplementary Fig. 5), as these are fundamental choices. The calibration procedure and the overall experimental workflow from design to analysis (Fig. 4) indicate the necessary steps before main data acquisition to ensure high-data quality and reproducibility. In addition, we offer a checklist of essential considerations at each stage in the process

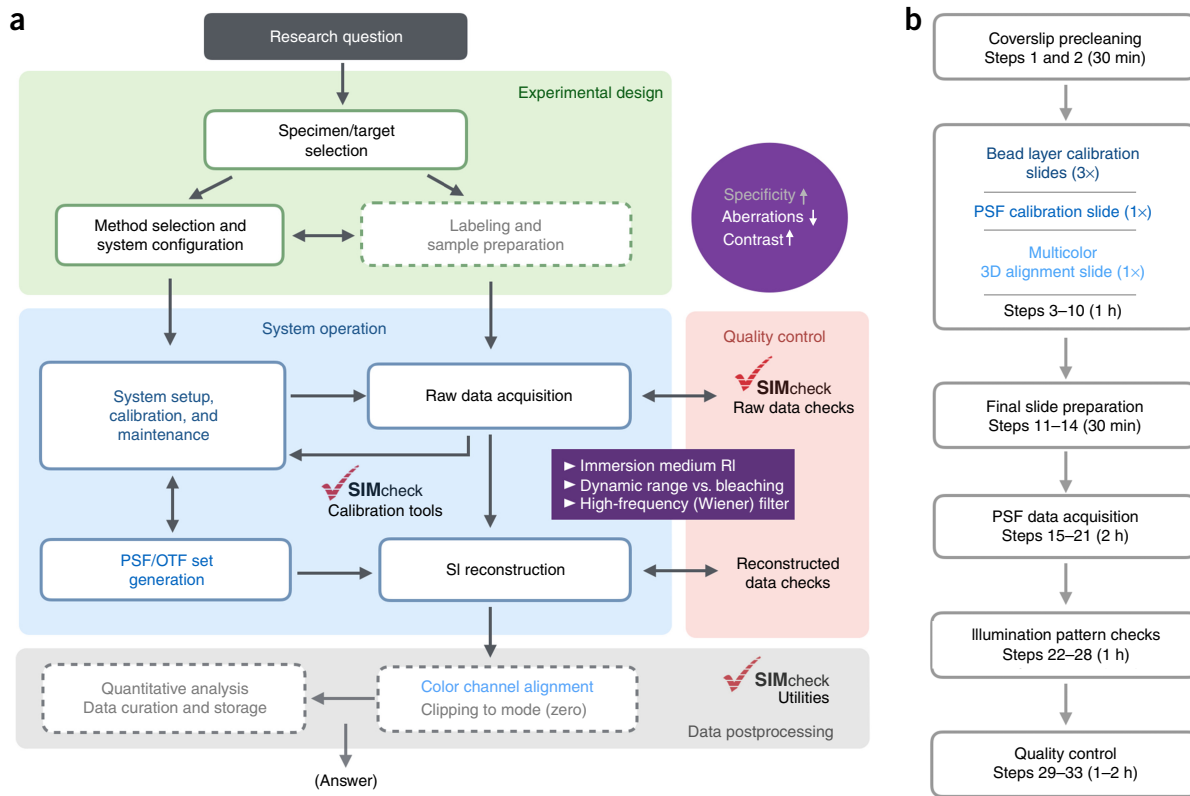


**Figure 4 |** Overview of the workflow for SIM experiments. **(a)** Workflow of the holistic SIM imaging process. Areas covered in this protocol are included in solid boxes, whereas areas covered in Ball *et al.*<sup>13</sup> and Kraus *et al.*<sup>15</sup> are included in dashed boxes. Central aims of the workflow are highlighted in the purple circle, and key points for the user to affect the imaging result are listed in the purple rectangle. Locations in the workflow where SIMcheck can be used are illustrated. More detailed checklists are provided in **Supplementary Figure 5** and in the **Supplementary Manual**. **(b)** Schematic of the procedure for assembling calibration slides and acquiring calibration data sets.

to facilitate experimental design refinement (**Supplementary Manual**) and provide a list of suitable fluorophores in **Table 1**.

The main procedure for assembling calibration slides and performing calibration checks is outlined in **Figure 4b**, and the slide preparation steps are illustrated in detail in **Figure 5**. The expected results from these calibration slides are shown in **Figure 6** and include selected examples of positive and sub-optimal outcomes, whereas recommendations for correcting errors in their preparation or imaging are listed in the Troubleshooting section. As RI mismatch is a primary cause of SIM artifacts, and perhaps the most easily adjusted system parameter, a guide to matching RI to immersion media, reconstruction OTF and sample is provided in **Figure 7**. Additional illustrations and in-depth information on this critical aspect are presented in **Supplementary Figures 6–9**. Further, an exhaustive list of SIM artifacts, their diagnostic readouts and potential countermeasures can be found in **Table 3**. For specialists and developers of bespoke SIM systems, we provide an additional list of artifacts and diagnostics that are mainly associated with basic system setup and initial light path alignments (**Supplementary Table 1**) and show a practical example of beam misalignment detection using SIMcheck (**Supplementary Fig. 10**).

To aid novices in their understanding of these concepts, a discussion of the fundamental principles of the SIM technique and image reconstruction in frequency space is provided in **Box 1** and **Figure 2**. Last, to work toward universal quality standards,

we include a set of guidelines and criteria for data presentation and publishing (**Box 2**). These are designed to help experimenters, principle investigators, reviewers and specialists involved in the publication process ensure transparency, consistency and reproducibility of the presented results. The protocol and recommendations are applicable to all commercially available and custom-built SIM systems, and add to the emerging range of open-source SIM-specific tools<sup>13,18,19</sup>.

### Level of expertise required

Any researcher or student familiar with generic wet-lab techniques and immunostaining may implement the calibration sample preparation protocol. No specific technical expertise is required to benefit from the experimental design and data presentation recommendations. Any researcher trained on a SIM instrument and familiar with recording data can implement the image acquisition, calibration data analysis and quality control recommendations. Training of individual users in system calibration protocols requires experience in optical microscopy and ideally advanced technical knowledge of the imaging platform.

### Limitations

Although this protocol should assist in improving the results of any SIM imaging experiment, it cannot overcome fundamental restrictions of the technique regarding resolution and photostability, or the limitations imposed by inherent properties of the

# PROTOCOL

**TABLE 1 |** List of recommended and less suitable fluorophores and fluorescent proteins for 3D-SIM applications.

Laser line	Recommended	Alternatives	Less suitable
405 nm	DyLight 405	CF405M, CF405S <sup>a</sup>	Alexa Fluor 405 <sup>b</sup>
488 nm	Alexa Fluor 488 <i>mNeonGreen</i>	ATTO 488, DyLight 488, <i>EGFP</i>	FITC
532 nm	Alexa Fluor 532	Alexa Fluor 555, Cy3	TRITC
561 nm	Alexa Fluor 568, <i>TagRFP</i>	Alexa Fluor 546/555, Cy3	Rhodamine Red, <i>mRFP</i>
592 nm	Alexa Fluor 594	ATTO 594, DyLight 594	Texas Red, <i>mCherry</i> <sup>b</sup>
640 nm	ATTO 647N		Alexa Fluor 647 <sup>b</sup> , Cy5 <sup>b</sup>

Note that the list is not exhaustive and that these recommendations are based on mounting in Vectashield. Fluorescent proteins are italicized.

<sup>a</sup>May photoconvert in other mounting media. <sup>b</sup>Not suited for mounting in Vectashield but reported to work well in other mounting media.

specimen or the biomolecular target of interest. While the 2D or 3D resolution increase provided by SIM is sufficient to resolve a range of biologically relevant macromolecular structures, any further increase in structural resolution—i.e., below ~100 nm—requires diffraction unlimited super-resolution approaches such as nonlinear SIM<sup>20–22</sup>, stimulated emission depletion (STED) microscopy<sup>23–25</sup> and single-molecule localization microscopy (SMLM—e.g., PALM, STORM)<sup>26,27</sup>. These modalities, along with lower-resolving techniques, such as wide-field deconvolution or confocal laser scanning microscopy, are alternatives to SIM that should be considered during the experimental design phase of a project. In the case of SIM providing sufficient resolution to address a given research question, it may prove advantageous over other super-resolution techniques because of its straightforward capabilities for multichannel, rapid, volumetric imaging, and thereby provide additional benefits (**Supplementary Fig. 5a**).

Finally, it should be noted that this protocol does not ensure success for every possible sample. Certain specimens and biomolecular targets are too difficult (due to size, diffractive properties, dispersion or label specificity) to image successfully even with these improved standards. Some biological and organic fluorophores do not have sufficient photostability to tolerate the repeated exposures of SIM (**Table 1**). As with all super-resolution techniques, a compromise must be reached for each application between photodamage, imaging speed, information content (wavelengths, 3D volume, sample size, number of time points) and spatial resolution (effectively contrast-limited), all confined by the available photon budget (**Supplementary Fig. 5a**, **Supplementary Manual**). In practical terms, finding the balance between contrast that is as high as possible (i.e., by increasing target-specific signal and/or by decreasing nonspecific background) and keeping acquisition bleaching rates acceptable is imperative for producing

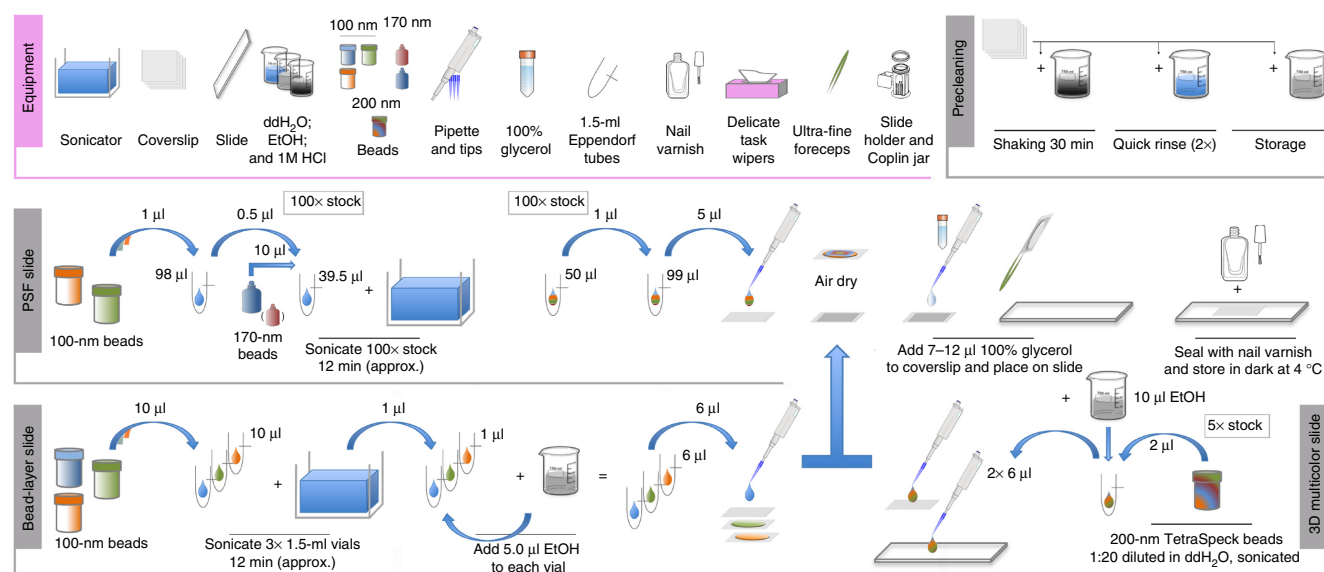


**Figure 5 |** Preparation of calibration bead slide set. An overview presenting the initial setup required before biological sample imaging, showing required materials and slide assembly steps, as explained in detail in the Procedure.

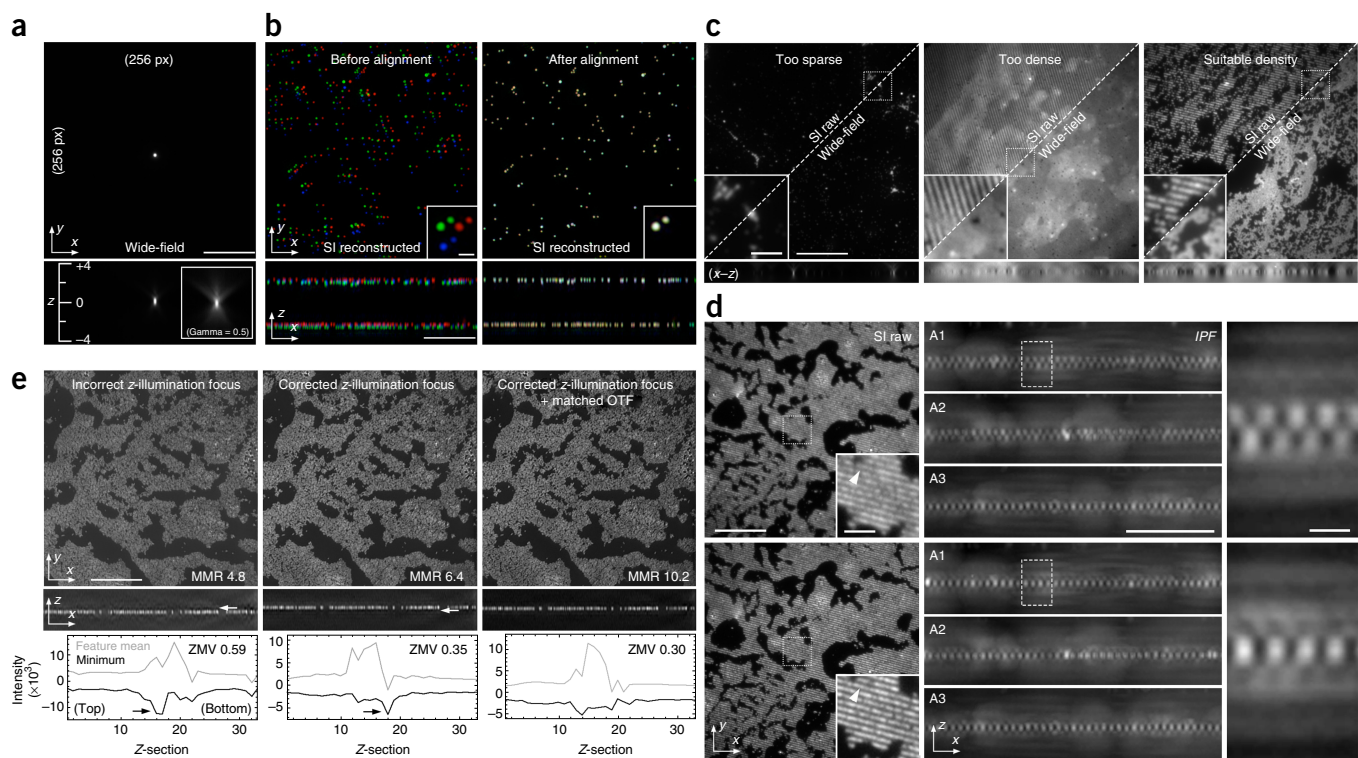


**Figure 6 |** Expected outcomes from calibration slide preparation. **(a)** PSF slides should provide well-distributed single beads attached to the coverslip surface to be recorded individually in a 256 × 256 pixel (px) frame, as shown here in wide-field mode. The orthogonal view of the bead is below, with axial depth indicated in microns on the x axis. The inset is displayed at the same scale, but with a gamma correction to illustrate the symmetry of the PSF and absence of any artifacts. **(b)** Expected outcome of 3D multicolor alignment slide, with a 200-nm-diameter TetraSpeck bead field shown before (left top panel) and after (right top panel) alignment with image registration software. The orthogonal views of each result are shown below. Note the axial separation of the two layers along the z axis, and the typical degree of channel separation illustrated in the top inset. **(c)** Outcomes from 100-nm-bead layer slides (green-emitting beads shown in SI and wide-field). Bead fields neither should have patches of beads that are too sparse (left) nor should the beads form very dense multilayers stacked on top of each other (middle). Ideal are intermediate-sized patches of bead monolayer interspersed by bead-free background areas (right panel). **(d)** Top panels show a bead field collected with reduced stripe contrast due to misalignment of the axial interference pattern; bottom panels show the correctly aligned axial interference pattern leading to improved stripe contrast. Left-most panels: representative single frame from raw data, with structured illumination pattern highlighted in inset, and arrowhead pointing to a typical instance of the pattern. Center panels: SIMcheck 'Illumination Pattern Focus' (IPF) module output, showing the orthogonal projection of resliced raw data in which the axial interference pattern is visible in the bead layer, for each illumination angle (A1 through A3). Right-most panels: inset from box in central panels showing a suboptimal 'zipper' pattern in the axial interference (top), and the desired pattern of axial interference (bottom), corresponding to the relative contrast of stripes as seen in the insets of the left-most panels. **(e)** Expected outcomes from bead-layer slides with combinations of suboptimal axial interference pattern (z-illumination) and suboptimal OTFs (collected with unmatched immersion medium RI), with corresponding 'Spherical Aberration Mismatch' plots (lower row). The left-most panel has both compromised z-illumination and incorrect OTF matching, and shows a low MMR value and a high z-minimum variance (ZMV) value (Fig. 3). The center panel has optimized z-illumination, but incorrect OTF matching, showing a higher MMR value and lower ZMV value. White arrows mark pronounced intensity dips below (left panel) or above (center panel) the bead field, also indicated by black arrows in the corresponding plots below. The right panel has optimized z-illumination and correct OTF matching, showing the highest MMR value and the lowest ZMV value, along with a total reduction of intensity dips around the bead field. Scale bars, 5 μm and 1 μm (insets).

high-quality SIM data (**Supplementary Fig. 5b**). Consequently, the limit of the method is reached if a minimum acceptable (modulation) contrast level is not achieved at all or is not achieved without exceeding the critical threshold for bleaching.

### Experimental design

The most fundamental prerequisite for the successful application of any advanced imaging approach, including SIM, is the appropriate experimental design for a given biological question (**Fig. 4a**, **Supplementary Manual**). Design considerations for the sample include the choice of the specimen, the biological target(s) to be imaged, labeling strategy, mounting medium and imaging controls. Thicker specimens (thicker than several tens of microns, such as whole-mount preparations or most tissue sections) are often impractical for SIM because of excessive spherical aberration,

light scattering and out-of-focus blur, limiting stripe contrast and hence the ability to extract super-resolved information. Importantly, not all biomolecular targets are suitable for current super-resolution imaging approaches; these include highly mobile or transient binding factors, which move too rapidly and have insufficient spatial specificity to be cleanly resolved after reconstruction. Furthermore, the structures of interest should be of the size or distance range to benefit from SIM's resolution increase. Many macromolecular complexes and structures, such as centrosomes or replication clusters, are in the size range of 100–200 nm and can be well resolved with SIM. Of note, distances between differentially labeled (multicolor) targets can be determined with an accuracy in the 10- to 20-nm range—i.e., far below the optical resolution limit imposed by the microscope<sup>15,28</sup>. On the other end of the scale, if the biological question does not require the

# PROTOCOL

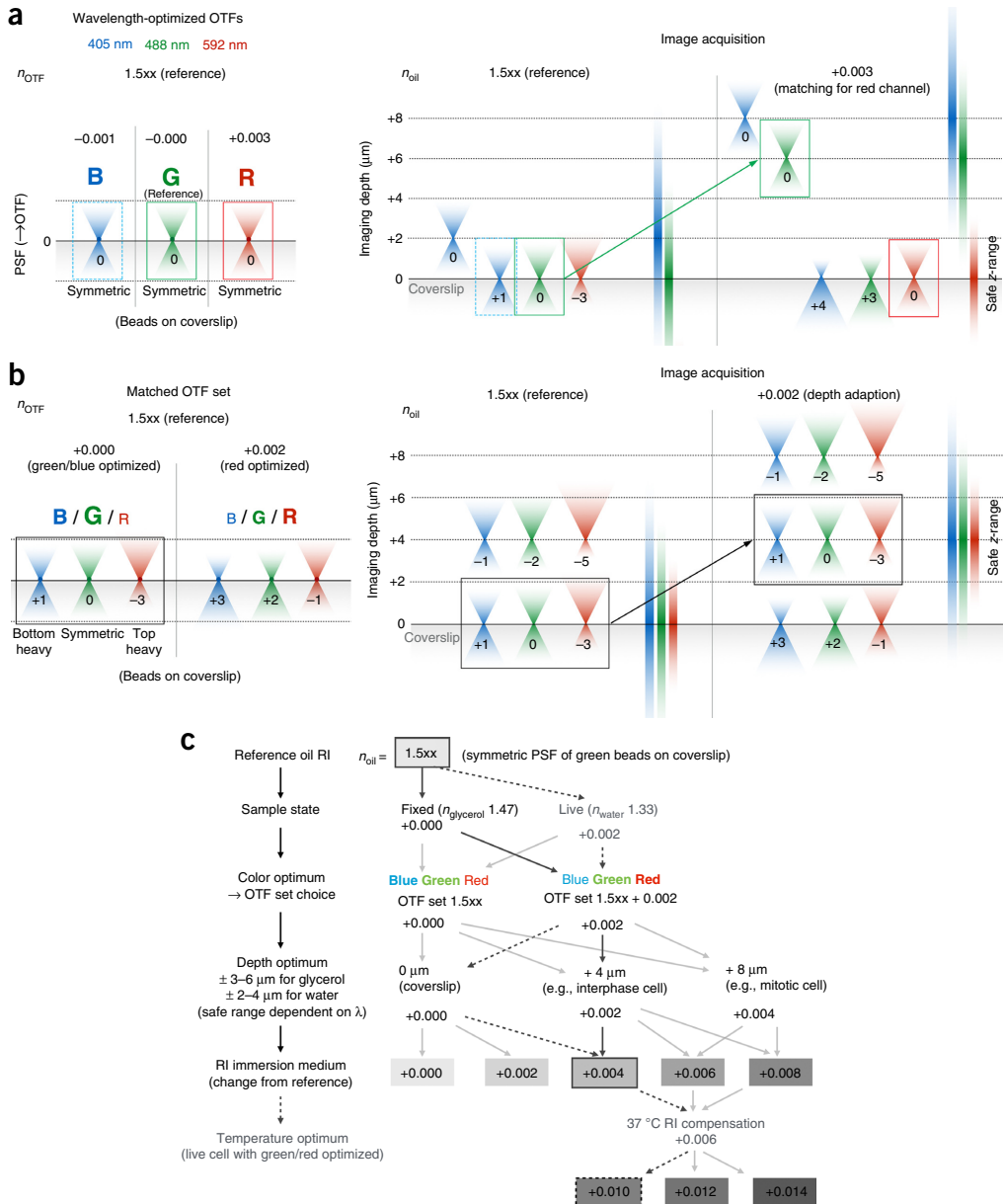


**Figure 7 |** Matching OTFs and experimental conditions in the sample for multicolor acquisitions. **(a)** Schematic representation of PSFs as a function of wavelength, depth, and immersion oil RI ( $n_{\text{oil}}$ ). Left panel: for the three displayed wavelengths, at a given reference value of the immersion oil RI, the PSF values (shown as hourglasses) will be horizontally symmetrical. If green is the reference channel, then the optimal RI for 405 nm will be 0.001 units reduced from the reference and the optimal RI for 592 nm will be 0.003 increased from the reference (e.g., 1.511 for 405 nm and 1.515 for 592 nm, with a 488 reference RI of 1.512). Right panel: during image acquisition using the green reference oil (e.g., 1.512), the point-spread behavior within the sample on the coverslip level will deviate (illustrated by the relative PSF shape). The blue PSF will become slightly asymmetric toward the coverslip (bottom-heavy), whereas the red PSF will become substantially top-heavy (the degree of asymmetry is indicated as the difference between the RI of the oil used and the channel-specific optimum RI, e.g. 1.512–1.515 = −0.003; hence it is given the index −3). Using a higher immersion-oil RI optimal for the red channel would match the PSF for the red channel for signals on the coverslip level but at the same time shift the optimums for blue and green deeper into the sample. Accordingly, the ‘safe z-range’ around the optimum (indicated by the vertical bars, narrowing with longer wavelengths), wherein SIM can be performed at minimal risk of spherical aberration artifacts, will be shifted. **(b)** Left panel: schematic of differences in PSFs of different wavelengths collected at the indicated immersion medium RIs, showing that OTFs collected at a given RI will always contain bias toward one channel or another—optimizing for any one channel brings a trade-off in other spectral ranges. Right panel: the effect of adapting the acquisition conditions of the OTF (boxed PSFs), on PSFs in the sample. Introducing an OTF set acquired with the same RI oil (optimized for either blue/green or red) unifies the ‘safe zone’ for a given set of wavelengths. These point-spread characteristics for all given channels can be adapted to the depth of interest by increasing the RI of the oil used for the acquisition (e.g., by ~4  $\mu\text{m}$  per 0.002 RI increase). **(c)** Workflow for selecting immersion-medium RI for both acquisition and OTF creation. On the left is a workflow diagram for determining the optimal immersion oil. Starting with the reference of an RI (1.5xx, where x is empirically determined for the system) that gives a symmetrical PSF for 488-nm beads on the coverslip, add or subtract the indicated RI for each subsequent choice, until arriving at the final RI for acquisition. This includes accommodations for the mounting medium, for which channel the OTF should be optimized; the optimal depth of the target structure; and any changes in temperature. With a reference RI of 1.512, following the solid black lines will give a result of an acquisition RI of 1.516, whereas following the dotted lines, with a different set of experimental criteria, will also give a value of 1.516 but for a different set of reasons. Other possible combinations are indicated by gray lines. Of note, the numbers and references given are empirically determined on a GE OMX V3 Blaze system, and may differ between manufacturers or among individual systems.

## Box 2 | Publishing guidelines

SIM is a highly complex method, and the increasing prominence of SIM data in biological publications—especially when it is included as one minor component of a larger study—poses a substantial problem because of the relative lack of experience of many users and manuscript reviewers. The requirement for (i) complex data processing using proprietary software and (ii) user-acquired system-specific calibration files (e.g., OTFs) adds to this burden. With this in mind, we suggest the following series of steps to ensure that data submitted, and eventually accepted for publication, are of adequate quality to justify deduced conclusions.

1. Representative raw and reconstructed data displaying the full 32- or 16-bit range (as appropriate) should be included as supplements or made otherwise available.
2. Raw data for the entire publication should be in a single, verifiable location, ideally a structured database such as OMERO<sup>46</sup>, easily producible upon request. These data should include not only raw image sets but also any associated calibration files, such as OTFs and image registration standards; otherwise, repeat processing will be impossible.
3. Discarding negative values in the reconstruction process (sometimes a default option in commercial software packages) must be avoided. Reconstructed data before image analysis or presentation should comprise the full dynamic range.
4. For main figures, thresholding of intensity values below 0, or the modal value, is acceptable, but should be noted in the (Supplementary) Methods section. When data contain a substantial contribution from label-free background, it is preferred to threshold intensity values to the mode value, rather than to 0, as reconstruction noise centers around the mode, whereas 0 may be variable in relation to the noise center between data sets.
5. Maximum-intensity projections must be clearly indicated as such.
6. Line profile plots of the unmodified reconstructed data through the structure of interest and neighboring background areas are recommended.
7. For multichannel studies, details of channel alignment (reference sample, software used, any other corrections) must be included in the (Supplementary) Methods.
8. Highly structured, iterative patterns (hexagons, triangles, repeated lines and so on) must be carefully scrutinized before being identified as biological structures, as many reconstruction artifacts have a similar appearance (regular polygons with angles equal to stripe rotations).
9. High-frequency noise filter settings (Wiener or other) used in the reconstruction software should be indicated in the (Supplementary) Methods.
10. The approach for OTF generation (user- or system-generated), and whether and how this is matched to the sample PSF, should be indicated in the (Supplementary) Methods.
11. The functional resolution (lateral and axial) of the system used should be assessed empirically through calculation of either full-width half-maximum of diffraction-limited structures or beads<sup>28</sup>, radial Fourier plots of reconstructed data<sup>13</sup> or Fourier ring correlation (FRC)-based methods<sup>47</sup>. The achieved resolution, rather than the theoretical resolution, should then be considered in the study before drawing biologically relevant conclusions.
12. Essential details on system configuration (if accessible) should be included:
  - System (make/model, any modifications)
  - Objectives (make, magnification, NA, correction and so on)
  - Laser lines (wavelength); potentially power, source, coupling (for bespoke systems)
  - Dichroic and emission filter sets
  - Camera settings/parameters (type, make/model, bit depth and so on)
  - Method (2D-SIM, 3D-SIM, TIRF-SIM and so on)
  - Acquisition modality (number of angles, number of phases, pixel size, z-step size and so on)
13. A general range of acquisition parameters (laser power, exposure time and so on) and reconstruction parameters (background offset, changes in default settings of apodization, filtering, or other parameters) should be included.
14. Quantification of signal distributions or proximity should accompany representative images.
15. Technical replicates of at least  $n = 10$  (e.g., cells on the same slide) and biological replicates of at least  $n = 2$  are recommended for qualitative or illustrative data. Technical replicates of at least ten and biological replicates of at least three are recommended for quantitative studies.
16. Perform a ‘reality check’. Are the biological conclusions (such as physical distances between protein factors) within the resolution range permitted by the system? Are any changes in distributions between targets affected by the channel alignment parameters? Can any unique or interesting patterns be explained by documented SIM artifacts before being attributed to a biological phenomenon?

extended resolution provided by SIM or other super-resolution methods (such as when analyzing nuclear versus cytoplasmic localization), then conventional imaging methods will be easier and better suited for the endeavor (**Supplementary Fig. 5a**).

Live-cell SIM imaging requires that the dynamics of the structure of interest be sufficiently slow as to preclude movement

during acquisition of one (3D) frame, as such movement could cause motion artifacts. Because of the relatively low photostability of fluorescent protein (FP) tags, trade-offs are inevitable in terms of z-resolution, the number of time points and multicolor imaging restrictions, and thus will affect the experimental design. It is noteworthy that the acquisition speed is markedly limited by the

## PROTOCOL

method of illumination pattern formation (in descending order of speed: galvonometer scanner array, spatial light modulator, mechanical grating) and the camera type (in descending order of speed: scientific complementary metal-oxide semiconductor (sCMOS), electron-multiplying charge-coupled device (EMCCD), charge-coupled device (CCD)) in different system setups. In this regard, the combination of 2D-SIM and total internal reflection fluorescence (TIRF) has been proven ideal for one- and two-color live-cell imaging of cell surface dynamics with very high frame rates, but at the expense of imaging in 3D and being restricted to the TIRF range of ~200 nm off the coverslip<sup>22,25,29</sup>.

**Hardware selection.** System hardware considerations cover mainly the choice of objectives, camera type or mode, filter sets and laser lines. As commercial system setups are typically restricted in the choice of components for different applications, various strategic decisions may have to be made when configuring a system for a desired application.

The standard oil-immersion objectives used for SIM should be independently checked for distortions of the PSF. High numerical aperture (NA) silicone oil-immersion objectives are superior for imaging larger z-volumes (beyond 10–15 μm in depth). The correction collar of these objectives must be adjusted precisely to allow matching of the imaging condition in the sample with the OTF set, analogous to changing the RI of the immersion oil (as discussed in detail below). Once set, as the RI of the mounting medium of the biological specimen (typically in the range of 1.37–1.39) is close to that of the silicone immersion oil (RI of 1.40), distortion effects from RI mismatches become negligible, and thus light scattering rather than spherical aberration becomes the limiting factor. The trade-offs in this case are reduced maximum resolution and brightness as a result of the lower NA of 1.30 (60×) or 1.35 (100×) silicone objectives as compared with traditional oil objectives with NAs of up to 1.42.

sCMOS cameras have significant advantages over CCD or EMCCD cameras regarding readout speed and field-of-view size. When camera readout speed is the limiting factor, sCMOS detectors are the superior choice for fast (live-cell) acquisition when combined with fast illumination pattern generation (via an SLM or galvonometer scanner array). The advantage of EMCCD cameras is the superior quantum efficiency and noise characteristics. Importantly, EMCCD cameras operated in conventional CCD mode are superior to sCMOS detectors in contrast-limited, but not photon-limited, imaging conditions. Such circumstances occur when densely labeled features extend within a larger volume in the axial direction, thereby strongly increasing out-of-focus blur (e.g., stained DNA in a cell nucleus). In comparison with sCMOS, the many-fold-larger well depth of CCD detectors allows a much higher dynamic range, increasing the modulation contrast in the image and ultimately improving the reconstructed data quality (**Fig. 3**). Finally, fast readout modes increase the camera readout noise and should be considered for only very fast live-cell imaging applications, as the disadvantage of higher detector noise for the reconstruction quality mostly outweighs the extra gain in speed.

The design and quality of dichroic mirrors and emission filters is critical not only for the detection efficiency and specificity, but also for structured illumination pattern generation. Poor design or damage can significantly affect pattern quality and consistency among various angle and phase positions.

The range of available laser lines is relevant to the versatility and application range of the SIM system. Of note, short wavelength excitation with 405 nm offers not only the advantage of a higher resolution (down to 90 nm in *xy*) but also features a broader ‘safe zone’ in the *z*-range, where ghosting artifacts from spherical aberration remain below a reasonable threshold (as discussed below). Using the calibration and OTF generation procedures described here, combined with labeling by sufficiently bright and photostable dyes (e.g., DyLight405 or CF405M/S), should overcome the current limitations of short wavelengths for fixed cell applications.

**Fluorophore selection.** 3D-SIM imposes less strict requirements on the photophysics of dyes than its counterpart super-resolution techniques, STED and SMLM. Hence, a wide variety of fluorophores and dyes have been successfully used in different SIM applications and systems. Despite being considered the least demanding among all super-resolution methods (by relying in principle on wide-field illumination and efficient CCD/CMOS detection, and not pushing resolution as much), SIM and particularly 3D-SIM still make a substantially higher demand on the available photon budget as compared with wide-field deconvolution microscopy, requiring up to 30-fold the number of acquisitions per 3D frame (5 phase steps, 3 angles, twofold *z*-sampling). Thus, the main criteria in fluorophore selection are brightness and photostability of the dye, as well as appropriateness for the laser line and filter set of the SIM system (**Table 1**). First-generation dyes such as FITC and TRITC are much more prone to bleaching and are not recommended. Careful selection of a mounting medium containing an antifade agent compatible with the chosen fluorophores is essential. Imaging of FP tags may be more difficult and depends on the expression levels, distribution and structure of the tagged protein to be imaged, with sample-specific out-of-focus blur levels often limiting contrast. For fixed-cell applications, the GFP signal can be enhanced with GFP-specific antibodies. Single-chain camelid antibody fragments (nanobodies) specific to GFP<sup>30</sup> and directly conjugated to more photostable dyes, such as ATTO 488 or Alexa 488, are useful because of their particularly high affinity and low background. The red fluorescent proteins mRFP and mCherry are typically too dim and bleaching-prone for 3D-SIM imaging without such post-detection. For live-cell applications, small self-labeling protein tags such as SNAP-tag or HaloTag can be superior alternatives if combined with tailored cell-permeable fluorescent or fluorogenic organic dyes<sup>30,31</sup>.

SIM imaging of far-red emitting dyes may demand an adapted system configuration to adjust the first-order beam positioning in the back aperture. In addition, some far-red fluorophores, such as Alexa Fluor 647 or Cy5, exhibit pronounced reversible dark-state switching in Vectashield<sup>32</sup> and thus require alternative mounting mediums (such as ProLong Diamond, under nonhardening conditions). Alternatively, if non-super-resolved wide-field information is sufficient, far-red dyes can be imaged in the conventional mode, deconvolved and overlaid with SIM images.

System configuration and acquisition order also affect how the sample is bleached. In particular, high-sensitivity detection allows for shorter exposure times, thereby reducing bleaching effects. Finally, acquiring full stacks for each angle consecutively (typical for systems using a rotating phase grating) is more prone

to bleaching artifacts than acquiring the stack with angles interlaced, per each z-plane (as in systems equipped with galvonometer scanner arrays or SLMs).

**Imaging controls.** Heightened technical standards will improve the final images from any experiment, but drawing meaningful conclusions from the data also requires appropriate controls. First, many studies seek to observe ‘colocalization’ of signals in two or more channels. However, super-resolution imaging has demonstrated that the concept of ‘colocalization’ is in many ways outdated; even when two targets are in biologically relevant spatial proximity, frequently signals will not overlap<sup>33</sup>. Therefore, multichannel colocalization or distance analyses should be supplemented by dual-color labeling of the same targets to provide technical baseline levels of signal separation<sup>34</sup>. Second, if possible, genetically encoded fluorophore localization should be confirmed with antibody labeling and vice versa, as a control for nonspecific background that can easily lead to false-positive signals. If the absolute number of targets or foci is important to the experiment, a control with a nonspecific fluorophore (such as only secondary antibody labeling or free GFP) can be used to establish a baseline for background signals. Third, as numerical quantification of imaging experiments is always preferred to illustrative single examples, a sufficient number of technical and biological replicates (generally no less than 10 and 3, respectively) should be analyzed. Finally, it is advisable for some applications to include fiducial markers of defined sizes, to compare with features of interest. Although this is challenging, recent protocols for DNA origami provide a useful example of highly customizable *in situ* controls for both absolute (single or multicolor) distance measurements and fluorophore density<sup>35</sup>.

#### System calibration and validation of system performance

For system calibration, we recommend the use of five separate calibration slides utilizing various types of synthetic fluorescent beads (**Figs. 5** and **6**). The first calibration slide presents a mix of up to four different color PSF beads in optimal density to accommodate convenient acquisition of channel-specific PSF/OTF sets acquired with the same immersion medium (**Fig. 6a**). Next, three (or more) slides present monolayers of ~100-nm (sub-diffraction)-diameter beads of different wavelengths matching the range of the system (i.e., 405 nm, 488 nm, 568/594/640 nm). Following the protocol below, these monolayers should be evenly distributed over the entire coverslip surface while leaving intermittent patches of bead-free background regions with a few isolated beads (**Fig. 6c**). These should be used as reference slides to determine system parameters (line spacing, stripe rotation ( $k_0$ ) angle), as well as to validate system alignment (phase and z-modulation; first- and second-order beam position) and system performance by measuring the practically achievable resolution, confirming stability of performance over time, and assessing the quality of new parameter settings or new OTFs. The final calibration slide is for 3D channel alignment with a dual-layer preparation of 200-nm-Tetra Speck beads attached at appropriate density to both the coverslip and the slide surface, separated by a layer of glycerol (**Fig. 6b**). Alternatively, multicolor click-labeled replication foci in mammalian cell nuclei can serve as an ideal biological calibration reference, and are described, along with ways to achieve optimal 3D color-channel alignment for multiple cameras using

open-source software solutions (e.g., Chromagnon; <https://www.github.com/macronucleus/chromagnon>), in a protocol by Kraus and colleagues also published in this issue<sup>15</sup>.

As previously outlined, maximizing modulation contrast is essential to generating high-quality SIM data. This begins with the structured illumination pattern generated by the microscope optics, and therefore system calibration is of paramount importance. Regular checks of system performance are necessary, as the pattern generation systems are delicate, and even minor disturbances in the optical path can have substantial effects on reconstruction quality. This spans rather technical concerns such as the alignment of the axial modulation maximum (hereby referred to as z-modulation) with the image plane (specific for 3D-SIM), to seemingly trivial issues such as dust on the optical components or fingerprints on the back of the objective. Once these issues are resolved, most artifacts can be localized to deficiencies in sample preparation or image acquisition.

The majority of SIM experiments are performed on commercial platforms from one of three suppliers: GE Healthcare’s OMX; Zeiss’s Elyra; or Nikon’s N-SIM systems. Although sharing the fundamental approach to SIM acquisition and reconstruction, each system (or in the case of OMX platforms, different versions) has a unique approach to both generating the structured illumination pattern and reconstructing data. These differences can result in system-specific artifacts and limitations, and should always be considered before starting a SIM imaging experiment. A useful comparison of commercially available SIM systems used with the same biological sample type is available<sup>36</sup>, but the type of system accessible will generally be out of the control of the average user.

Optimization of the imaging system is critical and includes characterizing the point-spread behavior of the system, temperature dependence, chromatic aberration and mechanical particulars such as stage drift or camera positioning. Although service engineers will set up, initially calibrate and annually maintain commercial SIM platforms, it is critical for advanced users or facility managers to perform basic calibration procedures independently and regularly check for performance drift over time. Moreover, procedures such as checking the uniformity and z-modulation of the illumination pattern, characterizing the PSF of the objective and checking reconstruction quality with bead samples are necessary for any new optical configuration, and should be performed regularly even with commercial systems to maintain consistency in data collection and provide evidence of suboptimal alignment in preparation for service visits.

**OTF generation and matching to sample acquisition.** SIM reconstruction algorithms use the OTF that mathematically describes the microscope’s response to a fluorescent point source (**Box 1**). Commercial SIM systems will visually represent the OTF in different ways, and provide different methods for OTF generation. Besides the general optical properties of the system (wavelengths, magnification, NA and so on), the OTF also encodes information on the level of spherical aberration and the modulation contrast of the structured illumination pattern. Thus, matching OTF and sample characteristics is a key goal in the acquisition process in order to keep artifacts below an acceptable threshold of detection (**Fig. 7**, **Supplementary Figs. 6–8**). There are several considerations for this process.

## PROTOCOL

First, spherical aberrations occur when light rays that strike a lens (or any other optical element) near the edge of the lens do not meet with rays passing through the center of the lens. Although most high-end microscope objectives are corrected for spherical aberrations, the corrections hold only under ideal conditions, including a coverslip thickness of 170  $\mu\text{m}$  and a perfect match of RI ( $n$ ) of the sample and the RI of the immersion oil (or immersion medium, if not oil) ( $n_{\text{oil}}$ ) (Supplementary Fig. 9a). Thus, the sample needs to be regarded as an integral part of the optical system. When spherical aberrations are minimized such that all light rays intersect in the same ‘diffraction limited’ spot, the respective PSF has a symmetrical hourglass appearance, when viewed axially (Fig. 6a). This shape will deviate under suboptimal conditions; it will become asymmetric toward the coverslip (bottom-heavy, if displayed in the orientation with coverslip at the lower end) if  $n_{\text{oil}}$  is higher than the optimum, and will become asymmetric in the other direction (top-heavy), if the  $n_{\text{oil}}$  is lower than the optimum (Fig. 7). It is important to understand how the PSF shape is altered with depth in different sample conditions, as this will determine where the PSF is optimally balanced and/or best matched with the respective OTF for reconstruction. To assess the behavior of PSFs at various depths and the effects on the reconstruction quality and the appearance of mismatch artifacts, we made use of (i) the dual-layer preparation of 200-nm multispectral beads (Supplementary Fig. 6) described above for 3D channel alignment and (ii) a dispersion of multispectral beads in a gel matrix (Supplementary Method). The latter is particularly useful to assess also the ‘safe zone’ of good reconstruction above and below the depth of the ‘optimal OTF match’—i.e., the range in axial depth where mismatch artifacts (‘ghosting’) are still acceptably low (Supplementary Fig. 7).

One important variable is the wavelength of the exciting and emitted light ( $\lambda_{\text{ex/em}}$ ) traveling to and from the fluorophore. Of note, instruments are typically calibrated for an intermediate excitation wavelength of 488 nm. Shorter and longer wavelengths will be diffracted at a smaller or wider angle, respectively. Hence, any optimization must include considerations of the laser line to be used, particularly for multicolor image acquisitions (Fig. 7). For any target away from the coverslip surface, as in most typical biological applications, the RI of the sample (or more specifically the biological specimen with its surrounding mounting medium) becomes a key factor: the larger the mismatch between the RI of the immersion medium and the RI of the sample, the larger the degree of aberration with increasing  $z$ -depth. As it affects the density and thus the effective RI of both oil and mounting medium, the temperature ( $T$ ) needs to be considered as well. Typically, the nominal RI of immersion oil is indicated for room temperature (23 °C), while deviations thereof decrease or increase the effective RI of the immersion oil if the temperature is higher (e.g., for live-cell observations) or lower, respectively (Supplementary Fig. 9b). The adverse effects can be compensated by either adapting the RI of the immersion oil or by changing the correction collar of the objective (if applicable).

Second, optical aberrations introduced by elements in the light paths, such as lenses and dichroic filters, affect the measured OTF, which can substantially deviate from a theoretical OTF based solely on the parameters of the objective. Hence, well-matched and empirically derived OTFs measured for individual channels will typically yield reconstruction results superior to those

of a theoretical OTF. Third, the effect of the  $z$ -modulation is also encoded in the reconstruction OTF, and is also dependent on the RI with which the OTF was recorded. This is why different combinations of RIs used for acquisition and reconstruction yield variable final results, with the higher mismatches generating worse reconstructions, as seen in a matrix of varying sample and OTF RIs (Supplementary Fig. 8). Instabilities of the  $z$ -modulation position over time should be monitored, and can be compensated for by measuring a newer, matching, OTF. Finally, high noise levels in the OTF will translate into a prominent high-frequency noise component in the reconstructed image, just as does high noise in the underlying data (Fig. 1b, Supplementary Fig. 1). Thus, it is important to acquire both PSF and sample raw data with a reasonably high dynamic range but without saturating the detector (ideally using >2/3 of the available CCD/sCMOS camera detector range). Laser power and camera exposure times for PSF and sample acquisition should be adjusted to achieve the optimal trade-off between high dynamic range and still acceptable photobleaching. Exposure times for fixed-cell applications should typically be in the range of 20–100 ms to reduce intensity fluctuations and avoid potential mechanical drift artifacts.

In conclusion, matching a data set acquired under less favorable sample conditions with an OTF that is acquired under the same suboptimal conditions will result in better reconstruction than using an OTF acquired under ‘ideal’ conditions (Fig. 7, Supplementary Figs. 6–8). This becomes particularly relevant when combining OTFs for multicolor acquisitions that will necessarily impose less favorable conditions for wavelengths away from the reference wavelength. The diagrams shown in Figure 7 and Supplementary Figure 9c–e provide general guidelines for how to adapt to different imaging conditions and different systems.

**Image reconstruction.** Given the robust (and often proprietary) nature of SIM reconstruction algorithms, the user’s ability to improve data post acquisition is relatively limited. However, the adjustment of certain parameters, most prominently the high-frequency noise (Wiener) filter, can compensate for underlying deficiencies in the raw data by reducing noisy high-frequency components in the reconstructed image. The optimal filter setting for a given data set can be estimated from the average modulation contrast to noise ratio (MCNR), one of several readout metrics of SIMcheck (Fig. 3, Supplementary Fig. 1). Other parameters may include a (typically autoestimated) weighting factor for the relative contribution of first- and second-order information to the reconstruction, camera offset (dark frame and gain correction) and apodization factor that adjusts the system’s input intensity profile. The angle directions ( $k_0$ ) and (second-order) stripe width of the illumination must be predefined, either as a starting parameter for an initial fitting and refinement procedure or optionally as a fixed parameter, if too few sample features or too little stripe contrast makes reliable fitting improbable. Incorrect parameter settings or fitting errors can cause severe ‘hatching’ artifacts in affected directions (Fig. 1c) and should be carefully monitored, typically through warnings in the reconstruction log file. Relevant reconstruction parameters should be documented (e.g., in a log file) to facilitate comparison of temporally distinct data sets. Perhaps the most common oversight in reconstruction is the discarding of negative values (thresholding) in the reconstructed data, which severely reduces the ability of the experimenter

to visually distinguish true signal from reconstruction artifacts (**Table 3**), and also deprives the user of the possibility of obtaining quantitative measures of the reconstructed data quality—e.g., through SIMcheck’s max-to-min ratio (MMR) or z-minimum variance (ZMW) metrics. Several methods of correcting for

artifacts computationally have been described, and these can improve image quality substantially<sup>18,37–41</sup>, but often at the expense of spatial resolution. Thus, to explore the full potential of the technique, there is no substitute for well-informed and thorough procedures at each step in the imaging process.

## MATERIALS

### REAGENTS

- Chloroform (Sigma-Aldrich, cat. no. 132950) **! CAUTION** Chloroform is hazardous. Avoid direct contact and inhalation.
  - Hydrochloric acid (37% (vol/vol); Sigma-Aldrich, cat. no. 258148) **! CAUTION** Hydrochloric acid is hazardous. Avoid direct contact.
  - Ethanol absolute (100% (vol/vol); Merck Millipore, cat. no. 100983) **! CAUTION** Ethanol is flammable.
  - Glycerol (>99.5% (vol/vol); Sigma-Aldrich, cat. no. 49770)
  - FluoSpheres carboxylate-modified microspheres, 0.1 µm, blue fluorescent (350/440; Thermo Fisher Scientific, cat. no. F8797)
  - FluoSpheres carboxylate-modified microspheres, 0.1 µm, yellow-green fluorescent (505/515; Thermo Fisher Scientific, cat. no. F8803)
  - FluoSpheres carboxylate-modified microspheres, 0.1 µm, red fluorescent (580/605; Thermo Fisher Scientific, cat. no. F8801), blue (360/440) and deep-red (633/660) PS-Speck beads, 0.17 µm diameter (PS-Speck Microscope Point Source Kit, Thermo Fisher Scientific, cat. no. P7220)
- Note: this manuscript uses ‘red’ and ‘far-red’, which are referred to in the Thermo Fisher PS-Speck Kit as ‘orange’ and ‘deep-red’, respectively. Alternatively, Fluoro-Max 0.10 µm blue fluorescent beads (Thermo Fisher Scientific, cat. no. B100B) may be used instead of blue (360/440) PS-Speck beads **▲ CRITICAL** For OTF generation, only these beads, among all tested alternatives, have the necessary photostability and brightness to avoid bleaching and create high-quality PSFs to use as input in OTF generation. Using conventional blue beads will result in lower-quality OTFs and thereby lower-quality reconstructions in the blue channel.
- TetraSpeck Fluorescent Microspheres, 0.2-µm diameter (Thermo Fisher Scientific, cat. no. T7280)
  - DV Immersion Oil Kit containing 1/4-oz. bottles of 18 oils with refractive indices 1.500–1.534 (GE Healthcare, cat. no. 29163068)
- Alternatively, Cargille Laboratories offers bulk ‘Laser Liquid’ customized to the RI requested

### EQUIPMENT

- Structured illumination microscope (e.g., GE Healthcare OMX, Nikon N-SIM, Zeiss Elyra S.1)
- Ultrasonic water bath sonicator (e.g., VWR Ultrasonic Bath)
- Fine-tip forceps (Dumont no. 5; Fine Science Tools, cat. no. 11251-20 or similar)
- Low-protein-binding 1.5-ml tubes with safe-lock lid (Eppendorf, cat. no. 022431081)
- Coplin jars (Thermo Fisher Scientific, cat. no. 107)
- Coverslip holder (mini-racks; ProSciTech, cat. no. H447)
- Soft task wipes (e.g., Kimwipes; Kimberly-Clark Professional, cat. no. 34155)
- Cotton-tipped swabs for optical cleanup (Edmund Optics, cat. no. 56-926)

## PROCEDURE

### Precleaning of coverslips and slides **● TIMING 30 min**

- 1|** Place coverslips in a mini-rack and preclean them for 30 min in a gently shaking beaker of 1 M HCl. Place slides in a Coplin jar and follow the same procedure.
  - 2|** Rinse twice in ddH<sub>2</sub>O, transfer to a beaker (a Coplin jar for slides) of 100% (vol/vol) EtOH and seal with Parafilm for storage. Air-dry and inspect before use.
- ▲ CRITICAL STEP** Thorough cleaning of coverslips is essential for preparing calibration bead slides. Dry slides and coverslips vertically or at an angle to avoid dust collection.
- PAUSE POINT** Precleaned coverslip can be stored for several months in 100% (vol/vol) EtOH in a suitable sealed container (e.g., Petri dish sealed with Parafilm) preferably at 4 °C to prevent evaporation.

- Lens-cleaning tissues (e.g., Whatman; GE Healthcare, cat. no. WHA2105862)
- Quick-drying nail polish, preferably bright colored metallic, or CoverGrip coverslip sealant (Biotium, cat. no. 23005)
- Borosilicate precision cover glasses, thickness no. 1.5H (170 ± 5 µm); 18 × 18 mm or 22 × 22 mm (e.g., Marienfeld Superior, cat. no. 0107032)
- Clean glass microscope slides (76 × 26-mm/cleaned and packed in fiber-free boxes, Menzel SuperFrost Plus; VWR, cat. no. 631-9483)
- Slide storage boxes (Pelco, cat. no. 2106)
- Computer (Unix or Windows 64-bit OS is preferred, with 32-bit systems acceptable but likely to show slow performance. Adequate storage capacities for the database setup are required, as well as 4–8 GB RAM and current multicore processors.)
- ImageJ (The Fiji distribution<sup>42</sup> of ImageJ<sup>43</sup> is recommended. Other ImageJ distributions must have the BioFormats Importer installed. All distributions should be the most up-to-date version.)
- SIMcheck plugin<sup>13</sup> for ImageJ/Fiji (The plugin should be installed for quality control and assessment of raw and reconstructed 3D-SIM data. For 3D FFT functionality in the most current SIMcheck 1.1 version (<https://github.com/MicronOxford/SIMcheck>), the Parallel FFTJ plugin (<https://www.sites.google.com/site/piotrwendykier/software/parallelfftj>) must be installed.)

### REAGENT SETUP

**1 M HCl** Add 7 ml of concentrated HCl to 250 ml of ddH<sub>2</sub>O. Store the solution at room temperature; it is stable for several months.

**70% (vol/vol) EtOH** Mix 15 ml of ddH<sub>2</sub>O and 35 ml of ethanol absolute in a 50-ml self-standing Falcon tube or suitable dispenser; the solution is used for microscope slide cleaning. Store it at room temperature; it is stable for several months.

**Chloroform** Prepare aliquots in 50-ml Duran glass bottles; it is used for microscope slide and objective cleaning. Store it at room temperature; it is stable for several months.

### EQUIPMENT SETUP

**Vortexes or sonicators** Benchtop vortexes and sonicators can be used interchangeably. However, if a water bath sonicator is used, monitor the water temperature, as it will rise over time and cause damage to carboxylate-modified beads.

**Structured illumination microscopy** The 3D-SIM system should be well aligned and calibrated by trained service engineers. For multicamera systems, a channel alignment sample should be prepared. Consistent temperature in the imaging room or environment (23 ± 5 °C, with <0.5 °C variation per hour) is recommended to avoid mechanical drift, variation in camera output and changes in the RI of immersion oil and samples.

## PROTOCOL

### Preparation of PSF calibration slide ● TIMING 60 min

▲ **CRITICAL** This section can be carried out concurrently with Steps 6 and 7 and 8–10.

▲ **CRITICAL STEP** Dilution ratios may have to be adapted depending on the microsphere manufacturer or microscope configuration.

3| Dilute 1 µl each of 0.1 µm 505/515 (green–yellow) and 580/605 (red) fluorescent carboxylate-modified microspheres in 98 µl of ddH<sub>2</sub>O to make a 100-µl prestock solution.

■ **PAUSE POINT** Diluted microspheres can be stored at 4 °C for several weeks.

4| Add 0.5 µl of the prestock solution, 10 µl of undiluted 0.17-µm 350/440 (blue) and 10 µl of undiluted 0.17-µm 660/680 (far-red) fluorescent carboxylate-modified microspheres to 29.5 µl of ddH<sub>2</sub>O to make 50 µl of the final stock solution.

■ **PAUSE POINT** The microspheres can be stored at 4 °C for several weeks.

5| Sonicate the final stock solution for 10 min. Dilute 1 µl of stock solution in 99 µl of EtOH. Immediately apply 5 µl of this solution to a precleaned coverslip, spreading the droplet with the pipette tip, and air-dry for at least 30 min. The final concentrations (1:10<sup>6</sup> for green/red microspheres, 1:500 for blue/far-red microspheres) are chosen to average slightly less than one bead per field of view (256 × 256 pixels; field size of ~20 × 20 µm with a pixel size of ~80 nm).

▲ **CRITICAL STEP** Homogenization of the bead solution can be achieved with vortexing. However, sonication is preferred, as it reduces the formation of aggregate pools as the beads dry.

▲ **CRITICAL STEP** Once the bead solution has been applied to coverslips, allow it to dry, undisturbed and covered for 30–60 min. Use before drying may cause the beads to detach.

### Preparation of bead-layer calibration slides ● TIMING 30 min (concurrent)

6| Sonicate 1 ml of undiluted 0.1-µm fluorescent carboxylate-modified microspheres and then transfer 1 µl to an Eppendorf tube. Use one tube each for blue, green–yellow, red and far-red microspheres.

7| Add 5 µl of EtOH absolute to each tube, depressing the pipette plunger once and immediately adding all 6 µl to the center of a precleaned coverslip. Use the pipette tip to spread the liquid from the center while the EtOH evaporates, without pipetting up and down. Air-dry for at least 20 min.

▲ **CRITICAL STEP** Work quickly. EtOH weakens the carboxylate-modified shells, and these microspheres will disintegrate if handled roughly or left in alcohol. In addition, the goal is to have contiguous patches of beads, ideally one bead-layer thick, to illustrate features of the structured illumination pattern. Spreading the microsphere droplet around the coverslip is critical to making flat patches of beads rather than clumps.

## ? TROUBLESHOOTING

### Preparation of 3D multicolor alignment bead slide ● TIMING 30 min

8| Dilute 0.2-µm-diameter TetraSpeck microspheres 1:20 in ddH<sub>2</sub>O and vortex them for 1 min.

▲ **CRITICAL STEP** To ensure even distribution of beads for image acquisition, thorough vortexing is critical. Alternatively sonicate for 10 min in an ultrasonic water bath.

9| Transfer 2 µl of the bead solution to an Eppendorf tube. Add 10 µl of EtOH absolute and, without delay, gently pipette 6 µl of the suspension onto the middle of a precleaned no. 1.5H coverslip from Step 2 and pipette 6 µl of suspension onto the center of a precleaned slide. Gently streak out the bead suspension on the coverslip and slide surfaces with the pipette tip.

10| Allow the beads to dry for at least 20 min covered and protected from dust. (Alternatively, if available, dry in a mini laboratory oven at 37 °C for 5 min.)

### Final slide preparation ● TIMING 30 min

11| For PSF and bead-layer calibration slides, apply ~10 µl of 100% (vol/vol) glycerol to the fully dried coverslip. Next, prepare a labeled and precleaned slide (frosting side down), or use nonfrosted slides.

12| Using a fine-tipped forceps, slowly lower the coverslip onto the slide, placing it at the center and taking care to avoid air bubbles.

**13** | Allow the glycerol to distribute evenly between the coverslip and the slide. Press down gently with a soft task wipe to remove excess mounting medium at the edges. Seal carefully with nail polish or coverslip sealant.

▲ **CRITICAL STEP** For 3D calibration slides, this will typically result in a distance of 5–10 µm between the two bead layers. Reducing the amount of glycerol to <10 µl may lead to the formation of air bubbles. Thus, if the distance between layers is larger, be more thorough in removing excess mounting medium at the edges. Thorough removal of excess medium also promotes hardening of the nail polish sealant, which is vital for long-term storage and repeated use of the sample.

#### ? TROUBLESHOOTING

■ **PAUSE POINT** Calibration slides can be kept for several days to weeks at 4 °C or for several months at –20 °C.

**14** | Before mounting calibration slides on the microscope, clean the coverslip surface with 70% (vol/vol) EtOH using soft task wipes, followed by 100% (vol/vol) chloroform, using an adhesive-free cotton swab or lens cleaning tissue.

#### Acquisition of PSF/OTF sets ● **TIMING 2 h**

**15** | Mount the PSF slide (Steps 3–5) using the reference imaging oil with an RI optimal for green emissions.

▲ **CRITICAL STEP** The reference RI for green emissions yields a symmetric PSF of green-emitting beads located on the coverslip. The reference RI for orange or red emissions is typically shifted by one oil step (+0.002) with respect to the green reference. Once the reference RI is determined for a given system and a given ambient temperature, it remains constant for those conditions. Note that temperature shifts affect the RI of immersion media and thus must be considered and appropriately corrected for (Fig. 7, Supplementary Fig. 9).

**16** | Find an area of the slide with isolated individual beads, and center a bead in the field of view such that no other beads are visible. The detector will report its highest count when the illumination focus is at the center of the bead. Incrementally adjusting the focus deeper/shallower into the bead (e.g., using z-steps of ~0.1 µm) will help to find the optimal midsection.

**17** | Acquire an 8-µm stack ( $\pm 4$  µm from the chosen bead center) with a step size of 0.125 µm in wide-field mode. Reviewing the intensity histogram of this stack, determine whether the acquisition's dynamic range has come as close as possible to the maximum bit depth of the camera (typically 14, 15 or 16-bit), without entering saturation. If saturated, reduce laser light intensity or exposure time as necessary, check that there is no saturation with a single acquisition frame and then acquire a new stack.

**18** | Assess wide-field PSF for any variation, asymmetry or astigmatism introduced by the objective or by air bubble(s) in the immersion medium by scrolling through the z-stack, as well as inspecting the orthogonal view. For better visualization of dim features in the PSF, such as Airy rings, use gamma scaling of 0.5 or lower (Fig. 6a).

#### ? TROUBLESHOOTING

**19** | Generate a series of OTFs from a bright bead using different acquisition angles. Assess the quality of each OTF visually (when possible) and empirically by reconstructing a bead layer data set recorded in the same channel with the same RI oil and acquisition settings (Steps 22–24). For quantitative comparison of reconstruction quality, use the MMR and ZMV metrics of SIMcheck (Step 29) (Fig. 6e). Repeat Steps 16–18 using the reference imaging oil with an RI optimal for orange/red emission as required.

**20** | Repeat Steps 15–19 for each objective as necessary.

**21** | When an optimal RI for the central wavelength has been determined, acquire a single-bead stack for OTF generation with the appropriate acquisition settings for the system in use (e.g., single-angle SI-PSF acquisition for OMX). This should be performed for all colors using the immersion oil with the RI that reflects the best trade-off in asymmetry between all channels, rather than using immersion oils with different refractive indices to acquire optimal PSFs for each channel. It is recommended that two OTF sets (multiple channel OTFs acquired with the same RI immersion oil) be generated: (i) using the reference immersion oil for the green channel, optimized for multicolor acquisition of blue and green fluorescence; and (ii) using the optimal immersion medium for the orange/red channel (i.e., the OTF set acquired with a higher RI immersion oil). Optimizing for the orange/red channel is recommended for multicolor acquisitions involving the red and/or far-red channel because of the larger range of safe reconstructions in the blue and green emission channels (Supplementary Figs. 7–9).

#### ? TROUBLESHOOTING

## PROTOCOL

### Illumination pattern checks ● TIMING 60 min

- 22| Mount the bead-layer slide for the given wavelength, using the reference imaging oil (Step 15; **Fig. 7**).
- 23| Find a field containing even bead monolayer patches with intermittent bead-free background areas and occasional single beads. Empty areas will be important for accurate clipping offset and for determining the sample's ZMV. Adjust acquisition parameters accordingly to use the recommended bit depth of the camera while avoiding saturation.
- 24| Acquire a stack (in structured illumination mode) of the bead field. Usually a stack height of 4  $\mu\text{m}$  is sufficient.
- 25| Visually inspect the raw data. It should be free of particularly dark corners, noticeable aberrations or extraneous patterns.
- 26| Open the raw data set in ImageJ/Fiji and use the 'Channel Intensity Profiles' tool in SIMcheck. Intensity should be near equal between phases (the spacing of data points) and roughly equal between angles (the difference between rows of data points). Some variation in intensity between angles is inevitable (because of factors such as single-mode vs. multimode fiber-optic coupling or transmittance/absorbance characteristics of the dichroic mirror) but should be under 30%.
- 27| With the raw data set enabled, select the 'Raw Data' > 'Fourier Projections' function in SIMcheck. Confirm the presence of distinct first- and second-order spots in the Fourier transform. Using the mouse cursor, hover over the spot farthest from the center; ImageJ/Fiji will report the achieved resolution in microns per cycle. Absence of spots from the SIMcheck readout may indicate that initial diffraction spots were beyond the radius of the system's back focal plane because of misalignment, leading to a low abundance of high-order information assigned to the spatial domain. Alternatively, because of the Stokes shift of excitation and emission wavelengths, second-order emission spots may escape the back focal aperture (e.g., if far-red excitation spots are positioned at the very edge of the aperture).
- 28| Apply the 'Illumination Pattern Focus' calibration tool in SIMcheck. If the channel-specific angle is known, enter this number. Otherwise, this angle can be derived from the raw data set itself by drawing a line selection parallel to the contrast stripes. What is produced is a projected orthogonal view of the stripe pattern for each angle to assess the position of the 3D illumination pattern relative to the image plane. The axial modulation of the illumination should be consistent in all three angles. Ideally the maximum stripe modulation should be in line with the bead layer, thus showing a single layer of alternating bright and dark square-like sections across the field, rather than appearing as a 'zipper-like' double layer (**Fig. 6d**).
- Reconstruction of calibration data sets and quality control ● TIMING 1–2 h**
- 29| Using the raw data collected in Step 24, and the channel-specific OTFs collected in Step 21, reconstruct the raw data using the commercial or open-source SIM reconstruction software of choice. For multicolor acquisitions (such as with experimental data sets), use a set of channel-specific measured OTFs acquired with immersion medium of the same RI  $n_{\text{oil}}$  (or  $n_{\text{silicone}}$ ) for all channels, optimizing either for the green/blue (two-color only) or for the red channel (for two- and three-color experiments including the red channel) as appropriate (**Fig. 7b**, **Supplementary Fig. 9**).
- 30| For the reconstruction processing of the calibration (as well as experimental) data sets, deactivate the option in the reconstruction software that ignores negative unsigned values in the image. This option is titled 'Discard Negatives' in GE's SoftWoRx and 'Baseline Cut' in Zeiss's Zen SIM reconstruction software.  
▲ **Critical STEP** SIMcheck reconstruction quality checks require nonthresholded (unclipped) data. Thresholding can be applied after quality control—e.g., using SIMcheck's 'Threshold and 16-bit Conversion' utility.
- 31| Empirically determine a high-frequency noise (Wiener) filter setting appropriate for the data, using the Wiener filter setting recommendation in SIMcheck's 'Raw Modulation Contrast' tool, if applicable.
- 32| Perform the spherical aberration mismatch check on the reconstructed data set in SIMcheck and assess the value of the ZMV statistic.
- 33| Assess reconstruction quality, check for artifacts (**Figs. 1 and 3**) and proceed to acquisition and reconstruction of experimental samples.

### ● TIMING

Steps 1–2, precleaning of coverslips and slides: 30 min

Steps 3–5, preparation of PSF calibration slides: 1 h

Steps 6 and 7, preparation of bead layer calibration slides: 30 min; can be concurrent with Steps 3–5

Steps 8–10, preparation of multicolor alignment bead slide: 30 min; can be concurrent with Steps 3–5

Steps 11–14, final slide preparation: 30 min

Steps 15–21, acquisition of PSF/OTF sets: 2 h (with practice)

Steps 22–28, illumination pattern checks: 1 h

Steps 29–33, reconstruction and quality control of calibration data sets: 1–2 h

### ? TROUBLESHOOTING

Troubleshooting advice for the preparation of bead slides and acquisition of calibration data can be found in **Table 2**.

An extended documentation and troubleshooting of various SIM-related artifacts is provided in **Table 3**. Troubleshooting advice for certain system alignment issues can be found in **Supplementary Table 1**.

### ANTICIPATED RESULTS

There are five (or more) calibration slides produced in this protocol: three (or more) dense-bead slides with single-wavelength beads for each channel of the microscope, one dilute-bead slide with multiple single-wavelength beads for acquisition of PSFs in multiple channels and one moderately dilute bead slide with multiwavelength beads for multichannel alignment.

The PSF slide should have single subdiffraction-sized (0.1–0.17 μm) beads, diluted sufficiently to obtain single beads per 256 × 256-pixel frame (**Fig. 6a**). This density allows for creation of experimental OTFs on GE systems; although other

**TABLE 2** | Troubleshooting table.

Step	Problem	Possible reasons	Solution
7	Floating debris in bead-layer slide	Bead-layer slide is either old or beads were not sufficiently dried before mounting, causing beads and monolayer fragments to detach and move inside the mounting medium	Prepare a new bead-layer slide. Dry beads longer and/or use a mini oven at 37 °C. Store in a cool, dry location when not in use. Keep it out of light, when possible
	Bead layer is too sparse	Beads dispersed too quickly to form monolayers	Increase the volume of undiluted bead stock solution. Use less ethanol when applying undiluted beads
	Bead layer is too dense	Beads were not dispersed quickly enough	Reduce the volume of undiluted bead stock solution. Increase the ethanol ratio applied with undiluted beads
13	Bubbles in mounting medium	Too little mounting medium applied Alternatively, the drop of mounting medium applied already contained bubbles when pipetted onto the coverslip	For a small single bubble: scout a new area of your sample until a PSF bead with uniform Airy rings can be found and acquired For larger and multiple bubbles: apply mounting medium to the center of the coverslip without creating any bubbles, and gently place the coverslip directly atop the droplet. The weight of the coverslip will allow the droplet to spread radially out toward the coverslip edges. Only after all edges have been reached, remove excess mounting medium with gentle pressure from fingers, clean and seal. Alternatively, place tiny strips of torn filter paper (Whatman no. 4) against each edge of the coverslip and leave them for a couple of minutes to wick away excess mountant
	Crescent-shaped Airy rings	Bubbles in immersion medium	Remove the slide, clean oil off the objective, first with dry lens paper, and then with lens paper soaked in chloroform. Clean the coverslip (first dry it, then add 70% (vol/vol) EtOH, and then chloroform) and re-apply oil
18	Suboptimal OTFs	PSF Airy ring contribution from multiple beads	Check slides for bead density to ensure an 8-μm-thick, 256 × 256-pixel window can acquire a single PSF bead. Acquire PSFs of solitary, bright beads at different angles, and then select the optimal OTF

## PROTOCOL

**TABLE 3 |** Artifact documentation.

Figure or reference	Artifact type	Possible cause	SIMcheck readout	Troubleshooting
1b, Supplementary Figure 1	High-frequency noise ('hammerstroke') pattern associated with lower-than-expected resolution improvement	Low modulation contrast in the raw data because of inherently low contrast of the structure of interest or high out-of-focus blur contribution; sample labeling that is too weak; signal intensities (dynamic range) that are too low; and high-frequency noise (Wiener filter constant is set too low)	Raw 'Channel Intensity Profiles': total intensity variation (TIV) >50% 'Reconstructed Intensity Histogram': Max-to-min ratio MMR <3 'Raw Modulation Contrast': Modulation contrast ratio (MCR) <6 (recommended) Wiener filter constant OMX >0.0050 Reconstructed 'Fourier Plots'	[Sample] Choose suitable biological target/structure; revise labeling strategy; use brighter, more photostable dyes; reduce background caused by nonspecific labeling and/or avoid autofluorescence by switching to orange/red dyes [Acquisition] Increase dynamic range by increasing either laser power or exposure time until photobleaching becomes limiting Reduce z-height, while making sure that first and last image planes are just out of focus (ideally no stripes should be visible) Choose the region with reduced out-of-focus blur. Minimize squashing of extended structures along the optical axis by avoiding hardening mounting media (e.g., Moviol or ProLong Gold) [System] If photostability and timing considerations permit, use camera mode with higher photon well depth (CCD > EMCCD > sCMOS); decrease gain (EMCCD); use lower readout speed [Reconstruction] Increase Wiener filter constant to reduce frequency support, matching to the lower raw data quality. Note: an overly high filter constant (OMX >0.0060) may generate hatch pattern artifacts and blurry images with reduced resolution
3b,d	Locally confined high-frequency noise ('hammer-stroke') pattern  Low axial (z) resolution	PSF/OTF recorded with too low SNR  Reduced stripe modulation contrast in confined sample areas with high out-of-focus blur contribution  First-order excitation beams are not positioned near the edge of the back focal plane (BFP) (Note: axial frequency support may also vary between objectives, most notably through differences in the NA as z-resolution scales with $NA^2$ )	OTF amplitude 'lobes' have frayed edges (OMX)  'Modulation Contrast Map'  'Raw Fourier Projection': Second-order emission spots (close to the BFP edge) should be clearly detectable on high-contrast (calibration) sample, with radial position near the outer frequency limit 'Reconstructed orthogonal Fourier Plots': Reduced $k_z$ -frequency support (corresponding resolution lower than 400 nm)	[System] Acquire channel-specific PSF/OTF with high dynamic range, while avoiding saturation or extensive exposure times (>200 ms). If beads are too dim, prepare new bead sample on thoroughly cleaned no. 1.5H precision coverslips mounted with pure glycerol  [Acquisition] Increase dynamic contrast in the raw data. If applicable, exclude image regions with substandard MCR from consideration/evaluation  [System] Test axial resolution of the objective by measuring the axial (xz) full width at half maximum (FWHM) of individual 100-nm beads (wide-field and reconstructed SIM) in different color channels If FWHM of reconstructed beads is substantially >350 nm, consider recalibration of the system (requires service engineer)

(continued)

**TABLE 3 |** Artifact documentation (continued).

Figure or reference	Artifact type	Possible cause	SIMcheck readout	Troubleshooting
	Low lateral ( <i>xy</i> ) resolution	One (or both) first-order beam is clipped off or lost by a TIRF effect (e.g., for longer wavelength and high RI mismatch with culture medium)	'Raw Fourier Projection': (see above) 'Reconstructed Fourier Plots': (lateral) Reduced $k_{x,y}$ -frequency support (>150 nm)	[System] Check centering of the beam: remove objective, open the shutter and project beams to a suitable surface at a 0.5–1.5 m distance—e.g., a white piece of paper adhered to the ceiling of the incubation chamber. Adjust illumination power as required. Mark the location of each angle's 0th order. (Caution: only to be performed by a trained specialist. Do not look directly at laser light!) If substantially off center, the system needs to be re-aligned (requires service engineer) Zeiss: Use coarser diffraction grids or a relay lens with a shorter focal length
1e, Supplementary Figures 3, 6 and 7	Refractive index mismatch artifacts  Intensity side lobes along the <i>z</i> -axis ('ghosting')	Mismatch between the assumed optical response of the system encoded in the OTF and the effective optical response in the sample region of interest for the specific wavelength and imaging condition  [Sample] Spherical aberration mismatch (i) by using an immersion medium with the wrong refractive index (RI) or operating at the wrong temperature, or (ii) if the sample (region of interest) is far from the coverslip or the coverslip thickness is wrong, or (iii) correction collar of the objective (if equipped with one) is set to the wrong position	'Spherical Aberration Mismatch': <i>z</i> -minimum variance (ZMV) is relatively high (>0.5–1, sample-dependent) One-sided shifted minima relative to mean intensity peak indicate mismatch Note: check requires suitable sample (flat, well contrasted; e.g. single-bead layer). Low <i>z</i> -minimum variance (ZMV) and balanced profile relative to mean intensity profile indicate good match	[Sample] Match optical properties of the sample and the OTF  [Acquisition] Adjust RI of the acquisition immersion oil (or use a correction collar) to correct for mismatch induced by imaging depth, sample/medium RI and temperature  [System] Ensure temperature stability Acquire new wavelength-specific OTFs to compensate for long-term system variations Test the quality of OTFs and matching to system calibration settings by acquiring and reconstructing bead layers
		[System] Grating position (distance to relay lens) or 'top phase' galvonometer scanner alignment (OMX Blaze)	[System calibration] 'Illumination Pattern Focus': Record dense 100-nm bead layer and test for balanced alignment of the illumination <i>z</i> -modulation with the focal plane in all angles	[System] Run 'Grating Calibration' utility (N-SIM) Adjust grating position or 'top phase' settings (OMX service technician only)

(continued)

## PROTOCOL

**TABLE 3 |** Artifact documentation (continued).

Figure or reference	Artifact type	Possible cause	SIMcheck readout	Troubleshooting
1d, Supplementary Figure 2	Stripes in either 1, 2 or all 3 angles ('hatching'). Reduced structural resolution in affected orientation	Incorrect angle ( $k_0$ ) used for the reconstruction Insufficient feature content and/or low modulation contrast does not allow reliable fit	'Reconstructed Fourier Plot': Frequency range extends less in the affected orientation(s), i.e., asymmetric 'flower pattern' if 1 or 2 angles are affected	[Reconstruction] Determine the correct $k_0$ values—e.g., by reconstructing dense bead layer or sample with dense, high-contrasted features (OMX: check SIR log file for issued warnings) If low feature content and contrast do not allow reliable $k_0$ fit, use fixed $k_0$ values (determined from bead layers)—OMX only
Ref. 13	Stripes in angle direction(s), restricted to very bright regions only	Oversaturation: Intensity-saturated regions in the raw data show no stripes (i.e., no interference).	'Modulation Contrast Map': Green color indicates oversaturated pixels in the raw data	[Acquisition] Reduce excitation light or exposure times to avoid oversaturation or exclude oversaturated areas from consideration/evaluation
Ref. 13	Stripes, locally confined	Movement of fluorescent particles, features or cells between acquisition of the different angles—e.g. floating antibody aggregates due to low affinity or poor sample preparation	'Motion & Illumination Variation': Spots/features with distinct cyan, magenta, yellow coloring	[Sample] Thoroughly wash, post fixation with 4% (vol/vol) formaldehyde; use different antibodies or FP-tagged protein If applicable, exclude affected areas from consideration/evaluation
	Global (unidirectional)	Motion blur of the specimen; movement between acquisition of each angle (live cell movements or stage drift)	'Motion & Illumination Variation': Coloring of all features with distinct directionality	[Acquisition] Increase acquisition speed, decrease intervals between angle acquisitions; use OMX Blaze
	Global (multi-directional)	False 'drift correction' setting (OMX)		[Reconstruction] Activate 'drift correction' (OMX with rotary phase grating); deactivate 'drift correction' (OMX Blaze)
Supplementary Figure 10	Stripes in axial direction (combined with lateral stripes in out-of-focus planes)	Center beam mis-alignment between angle directions	'Reconstructed Fourier Plot - lateral and orthogonal': Spots in 3D FFT allow detection of regular stripe pattern in the reconstructed data	[System] Beam re-alignment necessary (requires service engineer)
1f, Supplementary Figure 4	Six-point hexagonal repeat (or 'honeycomb pattern') can be found globally throughout or at specific, isolated areas of 2D-SIM images acquired with 2-beam interference (+1, -1)	Spatial, low-frequency contribution is missing from axial direction ('missing cone' problem)	'Reconstructed Fourier Plot': Frequency range is reduced in all directions (symmetrical, but shrunken 'flower edges' are observed, as compared with expected resolution)	[Acquisition] Reduce contribution of out-of focus-light via TIRF or shallow z-stack acquisition If possible, acquire stack using 3-beam interference (+1, 0, -1) in lieu of 2-beam interference (+1, -1) Reconstruct image using an algorithm able to fill in 'missing cone.' (Example: fairSIM, with 'Attenuation' function enabled (ref. 19))

(continued)

**TABLE 3 |** Artifact documentation (continued).

Figure or reference	Artifact type	Possible cause	SIMcheck readout	Troubleshooting
Supplementary Figure 4	Z-wrapping artifact: orthogonal coarse stripes and decreased contrast/resolution throughout reconstructed data set. Prominent echo signals of opposing z-ends	First/last frame(s) of a z-stack starts/ends in prominent in-focus sample structure. 3D-SIM algorithm ‘loops’ information from last to first slice to allow the Fourier processing to work, as it assumes infinite structures	NA	[Acquisition] Extend height of z-stack, such that the structure of interest is just out of focus in the first and last image planes (i.e., no stripes visible in the raw image)
6b	Channel misalignment	Chromatic aberration: system instability, tilted emission filter (multicamera system)	NA	[Acquisition] Make use of multicolor 3D alignment calibration slide (e.g., 2-layer 200 nm TetraSpeck beads) to determine alignment parameters

NA, not applicable.

systems may require slightly different data sets for OTF creation, isolated PSFs are essential to determining the relative aberration of channel-specific PSFs in different immersion media and imaging conditions. The multichannel alignment slide should have two parallel layers of intermediately dense TetraSpeck beads ~5–10 μm apart to compensate for depth-related chromatic aberration (**Fig. 6b**). The bead layer slides should be dense enough to have uninterrupted patches of beads adjacent to isolated individual beads (**Fig. 6c**, right), while not too sparse (**Fig. 6c**, left) or overly dense (**Fig. 6c**, center). Running the ‘Illumination Pattern Focus’ function in SIMcheck will produce a projected view of the lateral cross-section of the bead-layer slide along each angle in the raw data (**Fig. 6d**). This permits visual inspection of the modulation pattern, to confirm that all three angles show a consistent relative positioning of axial modulation and image plane (bead layer) to ensure matching with the OTF. If misaligned, a ‘zipper’ pattern is observable in the bead field (**Fig. 6d**, top) as compared with a single bead layer with high-contrast (lateral) modulation (**Fig. 6d**, bottom). Check for various artifacts as shown, and consult the Troubleshooting table to make appropriate adjustments before continuing on to image biological samples. The differences in reconstruction quality upon optimization of z-illumination (system-permitted) and optimized matching of OTFs (e.g., old and a newly generated) should be empirically and quantitatively determined by comparing reconstructions of bead layers and measuring MMR and ZMV metrics with SIMcheck (**Fig. 6e**). Finally, off-center beam misalignment can be identified by a hatched pattern in out-of-focus regions, leading to spurious spots in the corresponding 3D-FFT that can be generated with the ‘Reconstructed Fourier Plot’ function in SIMcheck 1.1 (**Supplementary Fig. 10**).

Note: Any Supplementary Information and Source Data files are available in the online version of the paper.

**ACKNOWLEDGMENTS** We acknowledge J. Neumann and M. Grange for technical support, and L. Ferrand of GE Healthcare for helpful discussion. The 2014 OMX User Meeting made notable contributions to the publication recommendations. We thank all colleagues who contributed to many discussions to shape this protocol. We are further indebted to H. Leonhard and I. Davis for their long-standing support. This work was funded by the Wellcome Trust Strategic Awards 091911 and 107457 supporting advanced microscopy at Micron Oxford. The OMX 3D-SIM system in the Rockefeller University Bio-Imaging Resource Center was funded by award no. S10RR031855 from the National Center for Research Resources. J.D. is supported by the NIH-Oxford-Cambridge Scholars Program. G.B. is supported by an MRC Next Generation Optical Microscopy Award (MR/K015869/1). A.M. is supported by JSPS KAKENHI grant nos. JP16H01440 (“resonance bio”), JP15K14500 and JP26292169.

**AUTHOR CONTRIBUTIONS** C.I., J.D., A.J.N., M.M., E.M., Y.M. and L.S. collected data and created figures. A.M., G.B., M.M. and I.M.D. provided technical

expertise and advice. All authors contributed to artifact documentation. J.D., C.I., A.J.N. and L.S. wrote the manuscript. A.J.N., Y.M. and L.S. conceived the project.

**COMPETING FINANCIAL INTERESTS** The authors declare no competing financial interests.

Reprints and permissions information is available online at <http://www.nature.com/reprints/index.html>.

- Heintzmann, R. & Cremer, C.G. Laterally modulated excitation microscopy: improvement of resolution by using a diffraction grating. *Proc. SPIE* **3568**, 185–196 (1999).
- Gustafsson, M.G.L. Surpassing the lateral resolution limit by a factor of two using structured illumination microscopy. *J. Microsc.* **198**, 82–87 (2000).
- Gustafsson, M.G.L. *et al.* Three-dimensional resolution doubling in wide-field fluorescence microscopy by structured illumination. *Biophys. J.* **94**, 4957–4970 (2008).

## PROTOCOL

4. Schermelleh, L. *et al.* Subdiffraction multicolor imaging of the nuclear periphery with 3D structured illumination microscopy. *Science* **320**, 1332–1336 (2008).
5. Sahl, S.J. *et al.* Comment on ‘Extended-resolution structured illumination imaging of endocytic and cytoskeletal dynamics’. *Science* **352**, 527–527 (2016).
6. Li, D. & Betzig, E. Response to comment on ‘Extended-resolution structured illumination imaging of endocytic and cytoskeletal dynamics’. *Science* **352**, 527–527 (2016).
7. Shao, L. & Rego, E.H. in *Fluorescence Microscopy* 213–225 (Elsevier, 2014).
8. Allen, J.R., Ross, S.T. & Davidson, M.W. Structured illumination microscopy for superresolution. *Chem. Phys. Chem.* **15**, 566–576 (2014).
9. Rego, E.H. & Shao, L. Practical structured illumination microscopy. *Methods Mol. Biol.* **1251**, 175–192 (2015).
10. Fiolka, R. in *Quantitative Imaging in Cell Biology* **123**, 295–313 (Elsevier, 2014).
11. Komis, G. *et al.* Superresolution live imaging of plant cells using structured illumination microscopy. *Nat. Protoc.* **10**, 1248–1263 (2015).
12. Engel, U. in *Quantitative Imaging in Cell Biology* **123**, 315–333 (Elsevier, 2014).
13. Ball, G. *et al.* SIMcheck: a toolbox for successful super-resolution structured illumination microscopy. *Sci. Rep.* **5**, 15915 (2015).
14. Terui, Y. Image processing for structured illumination microscopy. in 1–3 (IEEE, 2015).
15. Kraus, F. *et al.* Quantitative 3D structured illumination microscopy of nuclear structures. *Nat. Protoc.* <http://dx.doi.org/10.1038/nprot.2017.20>.
16. Young, L.J., Ströhl, F. & Kaminski, C.F. A guide to structured illumination TIRF microscopy at high speed with multiple colors. *J. Vis. Exp.* <http://dx.doi.org/10.3791/53988> (2016).
17. Turnbull, L. *et al.* Super-resolution imaging of the cytokinetic Z ring in live bacteria using fast 3D-structured illumination microscopy (f3D-SIM). *J. Vis. Exp.* e51469–e51469 (2014).
18. Křížek, P., Lukeš, T., Ovesný, M., Fliegel, K. & Hagen, G.M. SIMToolbox: a MATLAB toolbox for structured illumination fluorescence microscopy. *Bioinformatics* **32**, 318–320 (2015).
19. Müller, M., Mörikemöller, V., Hennig, S., Hübner, W. & Huser, T. Open-source image reconstruction of super-resolution structured illumination microscopy data in ImageJ. *Nat. Commun.* **7**, 10980 (2016).
20. Gustafsson, M.G.L. Nonlinear structured-illumination microscopy: wide-field fluorescence imaging with theoretically unlimited resolution. *Proc. Natl. Acad. Sci. USA* **102**, 13081–13086 (2005).
21. Rego, E.H. *et al.* Nonlinear structured-illumination microscopy with a photoswitchable protein reveals cellular structures at 50-nm resolution. *Proc. Natl. Acad. Sci. USA* **109**, E135 (2012).
22. Li, D. *et al.* Extended-resolution structured illumination imaging of endocytic and cytoskeletal dynamics. *Science* **349**, aab3500 (2015).
23. Eggeling, C. & Hell, S.W. in *Far-Field Optical Nanoscopy* 3–26 (Springer, 2014).
24. Müller, T., Schumann, C. & Kraegeloh, A. STED microscopy and its applications: new insights into cellular processes on the nanoscale. *Chem. Phys. Chem.* **13**, 1986–2000 (2012).
25. Shao, L., Kner, P., Rego, E.H. & Gustafsson, M.G.L. Super-resolution 3D microscopy of live whole cells using structured illumination. *Nat. Methods* **8**, 1044–1046 (2011).
26. Betzig, E. *et al.* Imaging intracellular fluorescent proteins at nanometer resolution. *Science* **313**, 1642–1645 (2006).
27. Liu, Z., Lavis, L.D. & Betzig, E. Imaging live-cell dynamics and structure at the single-molecule level. *Mol. Cell* **58**, 644–659 (2015).
28. Wegel, E. *et al.* Imaging cellular structures in super-resolution with SIM, STED and localisation microscopy: a practical comparison. *Sci. Rep.* **6**, 27290 (2016).
29. Fiolka, R., Shao, L., Rego, H.E., Davidson, M.W. & Gustafsson, M.G.L. Time-lapse two-color 3D imaging of live cells with doubled resolution using structured illumination. *Proc. Natl. Acad. Sci. USA* **109**, 5311 (2012).
30. Rothbauer, U. *et al.* Targeting and tracing antigens in live cells with fluorescent nanobodies. *Nat. Methods* **3**, 887–889 (2006).
31. Grimm, J.B. *et al.* A general method to improve fluorophores for live-cell and single-molecule microscopy. *Nat. Methods* **12**, 244–250 (2015).
32. Olivier, N., Keller, D., Rajan, V.S., Gönczy, P. & Manley, S. Simple buffers for 3D STORM microscopy. *Biomed. Opt. Express* **4**, 885–899 (2013).
33. MacDonald, L., Baldini, G. & Storrie, B. Does super-resolution fluorescence microscopy obsolete previous microscopic approaches to protein co-localization? *Methods Mol. Biol.* **1270**, 255–275 (2015).
34. Cerase, A. *et al.* Spatial separation of Xist RNA and polycomb proteins revealed by superresolution microscopy. *Proc. Natl. Acad. Sci. USA* **111**, 2235–2240 (2014).
35. Schmid, J.J. *et al.* DNA origami-based standards for quantitative fluorescence microscopy. *Nat. Protoc.* **9**, 1367–1391 (2014).
36. Marno, K. *et al.* The evolution of structured illumination microscopy in studies of HIV. *Methods* **88**, 20–27 (2015).
37. Schaefer, L.H., Schuster, D. & Schaffer, J. Structured illumination microscopy: artefact analysis and reduction utilizing a parameter optimization approach. *J. Microsc.* **216**, 165–174 (2004).
38. Shroff, S., Fienup, J. & Williams, D. OTF compensation in structured illumination superresolution images. *Proc. SPIE* **7094** <http://dx.doi.org/10.1117/12.791052> (2008).
39. Débarre, D., Botcherby, E.J., Booth, M.J. & Wilson, T. Adaptive optics for structured illumination microscopy. *Opt. Express* **16**, 9290–9305 (2008).
40. Righolt, C.H. *et al.* Image filtering in structured illumination microscopy using the Lukosz bound. *Opt. Express* **21**, 24431 (2013).
41. Wicker, K., Mandula, O., Best, G., Fiolka, R. & Heintzmann, R. Phase optimisation for structured illumination microscopy. *Opt. Express* **21**, 2032–2049 (2013).
42. Schindelin, J. *et al.* Fiji: an open-source platform for biological-image analysis. *Nat. Methods* **9**, 676–682 (2012).
43. Schneider, C.A., Rasband, W.S. & Eliceiri, K.W. NIH Image to ImageJ: 25 years of image analysis. *Nat. Methods* **9**, 671–675 (2012).
44. O’Holleran, K. & Shaw, M. Optimized approaches for optical sectioning and resolution enhancement in 2D structured illumination microscopy. *Biomed. Optics Exp.* **5**, 2580–2590 (2014).
45. Demmerle, J., Wegel, E., Schermelleh, L. & Dobbie, I.M. Assessing resolution in super-resolution imaging. *Methods* **88**, 3–10 (2015).
46. Allan, C. *et al.* OMERO: flexible, model-driven data management for experimental biology. *Nat. Methods* **9**, 245–253 (2012).
47. Nieuwenhuizen, R.P.J. *et al.* Measuring image resolution in optical nanoscopy. *Nat. Methods* **10**, 557–562 (2013).